National Renewable Energy Laboratory

Innovation for Our Energy Future

Characterization of the Electronic and Chemical Structure at the Thin Film Solar Cell Interfaces

June 2005 – June 2009

C. Heske
University of Nevada, Las Vegas
Las Vegas, Nevada

Characterization of the Electronic and Chemical Structure at the Thin Film Solar Cell Interfaces

June 2005 – June 2009

C. Heske
University of Nevada, Las Vegas
Las Vegas, Nevada

Available electronically at http://www.osti.gov/bridge

Available for a processing fee to U.S. Department of Energy
and its contractors, in paper, from:
     U.S. Department of Energy
     Office of Scientific and Technical Information
     P.O. Box 62
     Oak Ridge, TN 37831-0062
     phone: 865.576.8401
     fax: 865.576.5728
     email: mailto:reports@adonis.osti.gov

Available for sale to the public, in paper, from:
     U.S. Department of Commerce
     National Technical Information Service
     5285 Port Royal Road
     Springfield, VA 22161
     phone: 800.553.6847
     fax: 703.605.6900
     email: orders@ntis.fedworld.gov
     online ordering: http://www.ntis.gov/ordering.htm

Summary

This project was devoted to deriving the electronic structure of interfaces in Cu(In,Ga)(S,Se)$_2$ and CdTe thin film solar cells. By using a unique combination of spectroscopic methods (photoelectron spectroscopy, inverse photoemission, and X-ray absorption and emission) a comprehensive picture of the electronic (i.e., band alignment in the valence and conduction band) as well as chemical structure can be painted. The work focused on (a) deriving the bench mark picture for world-record cells, (b) analyze state-of-the-art cells from industrial processes, and (c) aid in the troubleshooting of cells with substandard performance.

First funds for this project became available in the middle of July 2005. After that, the workforce of the group was expanded to the size required for this project. The necessary experimental instrumentation at UNLV was commissioned and contacts within the Thin Film PV Partnership Program (TFPPP) were established to secure a supply of adequate samples, even well beyond the official termination of the TFPPP on 9/30/2006. Samples were analyzed both in the lab at UNLV as well as during our experimental campaigns at the Advanced Light Source, Lawrence Berkeley National Laboratory.

Most recently, we have investigated the chemical and electronic surface structure of the current world record (20.0%-efficient) Cu(In,Ga)Se$_2$ (CIGSe) thin film solar cell absorber and the corresponding CdS/CIGSe interface of samples provided by the National Renewable Energy Laboratory (NREL). For the 20.0%-efficient CIGSe absorber, our measurements reveal that the surface composition is more Cu-deficient compared to less efficient absorbers and that the respective position of the conduction band minimum is comparatively shifted further away from the Fermi energy. Furthermore, we find a valence band offset of -0.90 (±0.15) eV and (as expected for a high-efficiency solar cell device) a flat conduction band alignment.

To investigate whether the composition of Cu(In,Ga)(S,Se)$_2$ (CIGSSe) chalcopyrite absorber has an impact on the formation of the Cu-poor, E_g-widened region and its extension into the absorber bulk, different chalcopyrite thin film solar cell absorbers provided by the Institute of Energy Conversion (IEC), University of Delaware were investigated. Our photon and electron spectroscopies were able to gain *depth-dependent* E_g information. For all investigated samples we find an increasing band gap energy with decreasing information depth and the formation of a surface region with significantly higher E_g. In addition, we find that the E_g-widened surface region extends further into the bulk of the absorber for the sulfur-free CIGSe absorber (i.e., the absorber with smaller bulk band gap) than for the CIGSSe absorber.

In addition to our investigations of the chemical and electronic surface structure of CIGSSe absorbers, we also studied the deeply buried CIGSSe/Mo interface. For the first time, we could draw a complete picture of the chemical and electronic properties of that interface. For these experiments CIGSe and CIGSSe/back contact samples were used, again prepared by the IEC group. We found a pronounced chemical interaction between absorber and back contact, namely the formation of MoSe$_2$ (and Mo(S,Se)$_2$) and a "diffusion" of Ga into the Mo layer. In addition, we could derive a flat valence band alignment at this interface.

Besides our studies on chalcopyrite thin film solar cell absorbers, we also investigated the chemical and electronic properties of structures relevant for CdS/CdTe-based thin film solar cells. Our results suggest that the CdS/CdTe interface is heavily intermixed, in particular after the $CdCl_2$ treatment. Efforts are still ongoing to reveal the electronic structure at that interface.

In order to shed light on the chemical and electronic structure in *real-world industrial-grade* samples, i.e., manufactured in large-scale, high-throughput equipment in an industrial environment, we have also studied selected samples (both, front and back sides) directly taken out of Global Solar Energy, Inc. ("GSE") production process after each preparation step. GSE has pioneered a unique robust process to manufacture CIGSe solar cell devices which can hardly be simulated on laboratory scale. While other companies pursue the approach of in-line deposition on rigid glass substrates, GSE is the only company to date using a roll-to-roll coating of the complete solar cell thin film layer stack on flexible substrates. Upon CIGSe formation our data shows that the back side exhibits $MoSe_2$ and absorber related XPS features. Compared to the front side, we find an increased amount of Ga on the back side which suggests a pronounced interaction with the front side upon roll-up.

Detailed Description of the Activities:

1. Establishing the group at UNLV

First funds for this project became available in the middle of July 2005. The initial activity was devoted to the expansion of the leadership work force for this project. With the arrival of Dr. Marcus Bär, a post-doctoral fellow (recipient of the prestigious German Emmy Noether Scholarship of the Deutsche Forschungsgemeinschaft) in mid-August 2005, and of Dr. Lothar Weinhardt, in January 2006, this expansion was fortunately very fast and successful.

Dr. Bär performed the research for his doctoral thesis at the Hahn-Meitner-Institut in Berlin, Germany, specializing in the optimization of interfaces between novel buffer layer materials and $Cu(In,Ga)(S,Se)_2$ thin film solar cell absorbers by chemical surface pretreatments. At UNLV, his primary focus was on modifying interface properties for an optimization of thin film solar cells with wide-gap chalcopyrite absorbers. Dr. Weinhardt, who came from the University of Würzburg, Germany, has pioneered the combination of UV- and Inverse Photoemission for the routine study of band alignment at thin film solar cell interfaces, as well as the to-date least intruding cleaning method for air-exposed thin film chalcopyrite surfaces (50 eV Ar^+ ion treatment). Both post-docs brought significant expertise in optimization and analysis of surfaces and interfaces in thin film solar cells into this project and have jointly led the TFPPP activities of the UNLV group. After Dr. Weinhardt and Dr. Bär left UNLV (at the end of 2007 and 2008, respectively) to start their own groups in Germany, Sujitra Pookpanratana (a graduate student from UNLV) took over UNLV's TFPPP activities.

2. Establishing a spectroscopic "tool chest" at UNLV

For the proposed characterization of the chemical and electronic surface and interface structures in thin film solar cells the necessary soft x-ray and electron-based spectroscopes needed to be established at UNLV.

During the course of this project, x-ray and UV photoelectron spectroscopy (XPS, UPS) was routinely used to investigate the chemical and electronic (occupied states) structure of the thin film solar cell samples. For the investigation of unoccupied states, inverse photoemission measurements (IPES) were conducted. The ultra-high vacuum (UHV) apparatus for these lab-based XPS/UPS experiments at UNLV was successfully commissioned and optimized for routine investigations after its relocation from the University of Würzburg, Germany during Spring/Summer 2005. During the last quarter of 2005 also the IPES setup was successfully included, such that first IPES spectra of reference samples could already be recorded by the end of 2005. Fig. 1 shows the first Fermi edge (of a Ag calibration sample) measured with our setup (open circles). The red line represents a fit of the spectrum which is used to derive the Fermi energy and in addition gives the total energy resolution of our setup (440 meV).

With funds from a different project, we were able to replace the old ESCALab MkII electron analyzer of our surface/interface characterization system, which showed reappearing electronic shortage problems in the first quarter and electronic communication problems in the second and third quarter of the first project year, by a high-performance state-of-the-art instrument (SPECS PHOIBOS150 MCD) in April
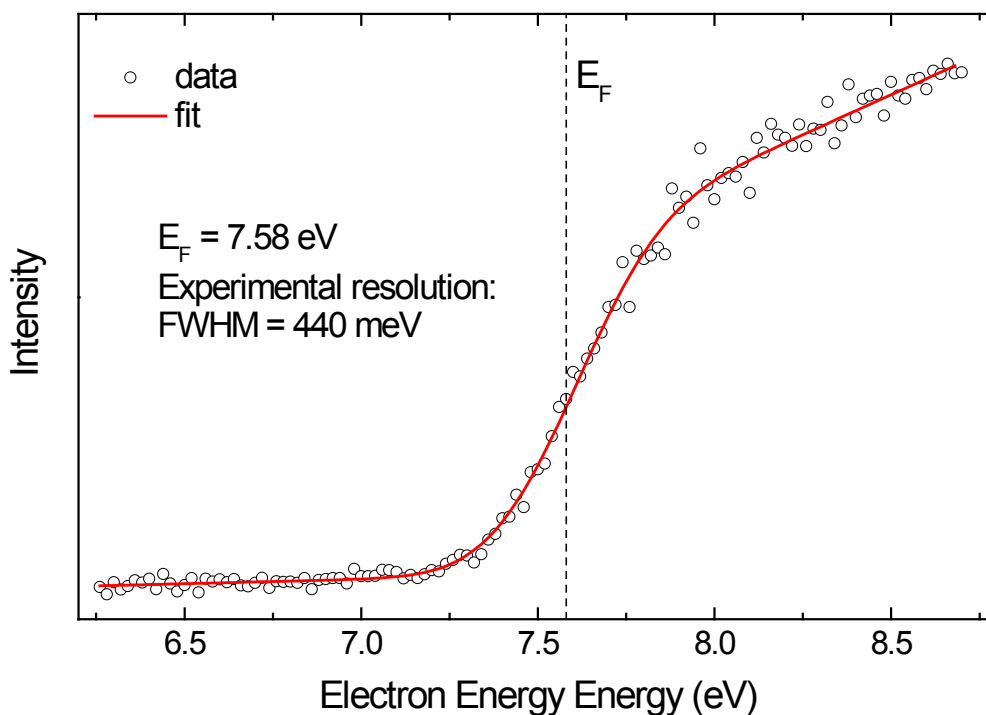
Fig. 1 *First inverse photoemission spectrum at UNLV (open circles). The red line represents a fit of the experimental data. The derived Fermi energy is given by the dashed vertical line.*

2006. After a downtime of only two weeks the new electron analyzer was commissioned and put to normal operation. The increased spectral resolution and an improvement of the signal-to-noise ratio in XPS by about two orders of magnitude greatly benefited the XPS and UPS results of our project and significantly reduced the experiment times. During the course of this project, we also replaced the old x-ray source by a high-performance state-of-the-art new x-ray source (SPECS XR-50), which again decreased the downtime of our surface analysis system due to maintenance issues and hence improved our sample throughput. For routinely performed XPS (UPS) measurements, we used Mg K_α or Al K_α (He I/He II) excitation and our PHOIBOS 150 electron analyzer with a multi-channeltron detector. The IPES experiments were conducted with a low-energy electron gun (STAIB) and a Dose-type detector with a SrF_2 window and Ar: I_2 filling were used. The experiments were performed in UHV with a base pressure below $1 \cdot 10^{-10}$ mbar.

In 2006, we also added a N_2-purged glovebox to our surface analysis system in order to minimize the exposure to ambient air of samples sent by our TFPPP collaborators to UNLV, which was critical for our surface-sensitive XPS, UPS, and IPES characterization. Usually the samples were individually packed in two plastic bags filled with dry nitrogen and some desiccant immediately after preparation in the labs of our collaborators. The sample exposure time to ambient air (before the first characterization) could thus be drastically minimized. Once at UNLV, the samples were unpacked in our glovebox under dry nitrogen atmosphere and directly introduced into our UHV surface characterization system.

Due to funds available from different projects, we could add a high-resolution XPS/UPS surface analysis system to our existing high-dynamic range measurement setup in 2007. This enabled us to investigate the thin film solar cell samples with much higher XPS and UPS spectral resolution (when necessary). Fig. 2 shows the development of our surface analysis system at UNLV during the course of this project.

In addition to the characterization of the thin film solar cell samples by these surface-sensitive, electron-based spectroscopies, we also used soft x-ray based techniques [x-ray emission (XES) and absorption spectroscopy (XAS)] for our studies. Due to the fact that these spectroscopies (XAS in fluorescence yield) are "photon-in-photon-out" techniques, their information depth is not limited by the inelastic mean free path of electrons but by the attenuation length of the soft x-rays in the probed material. Hence, the information depth is increased from a few nm (for XPS, UPS, and IPES) to several 10 nm up to a few 100 nm. These measurements were performed at the Advanced Light Source (ALS, Lawrence Berkeley National Laboratory). For the XES (XAS) measurements, we used the permanently installed SXF spectrometer of Beamline 8.0 (a channeltron mounted in front of the sample). Fig. 3 shows a picture of Beamline 8.0 with the SXF spectrometer.

In the last two project years, we (in close collaboration with Würzburg University) also designed and commissioned our own endstation at the ALS. The SALSA (Solid And Liquid Spectroscopic Analysis) endstation equipped with a high throughput and high transmission VLS (variable line spacing) soft x-ray spectrometer enabled us also to measure thin film solar cell samples more efficiently and with a higher signal-to-noise-ratio. A picture of the SALSA endstation is presented in Fig. 4.
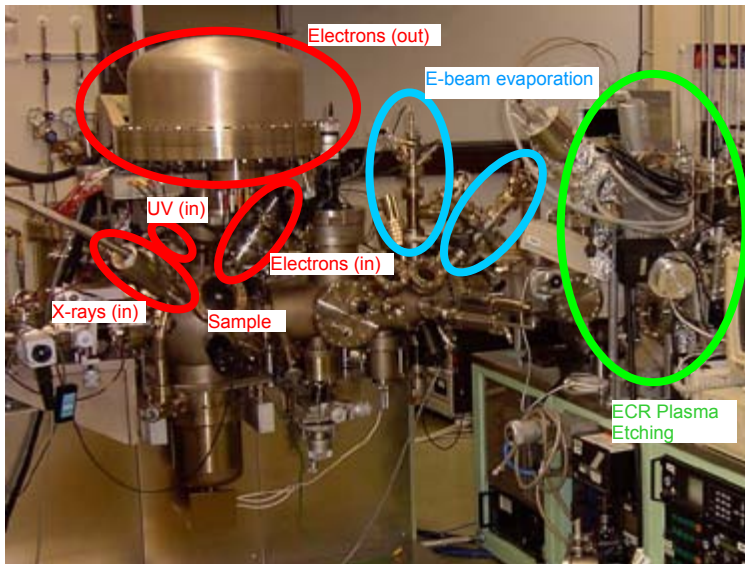
Fig. 2 *Picture of the ultra-high vacuum surface analysis instrument (a) still at Würzburg University, Germany and (b) after relocation to UNLV. Note the already replaced electron analyzer (red circle), the IPES setup (blue circle) and a scanning probe microscope (purchased with funds from a different project; green circle). (c) Current status of the surface analysis system at UNLV.*
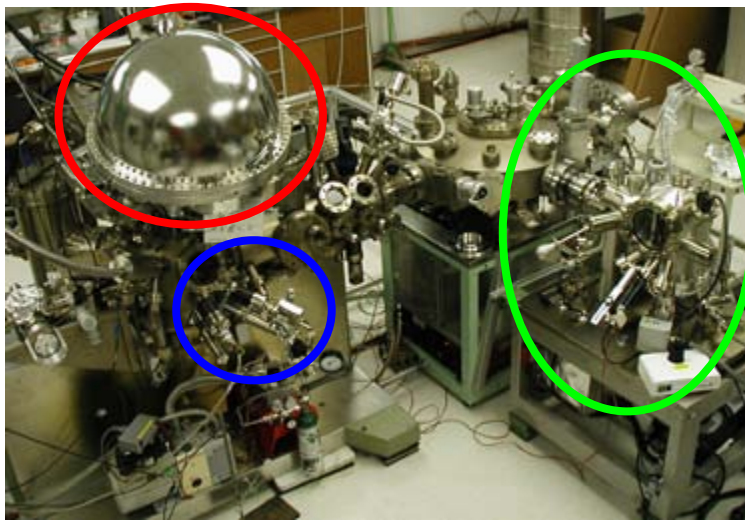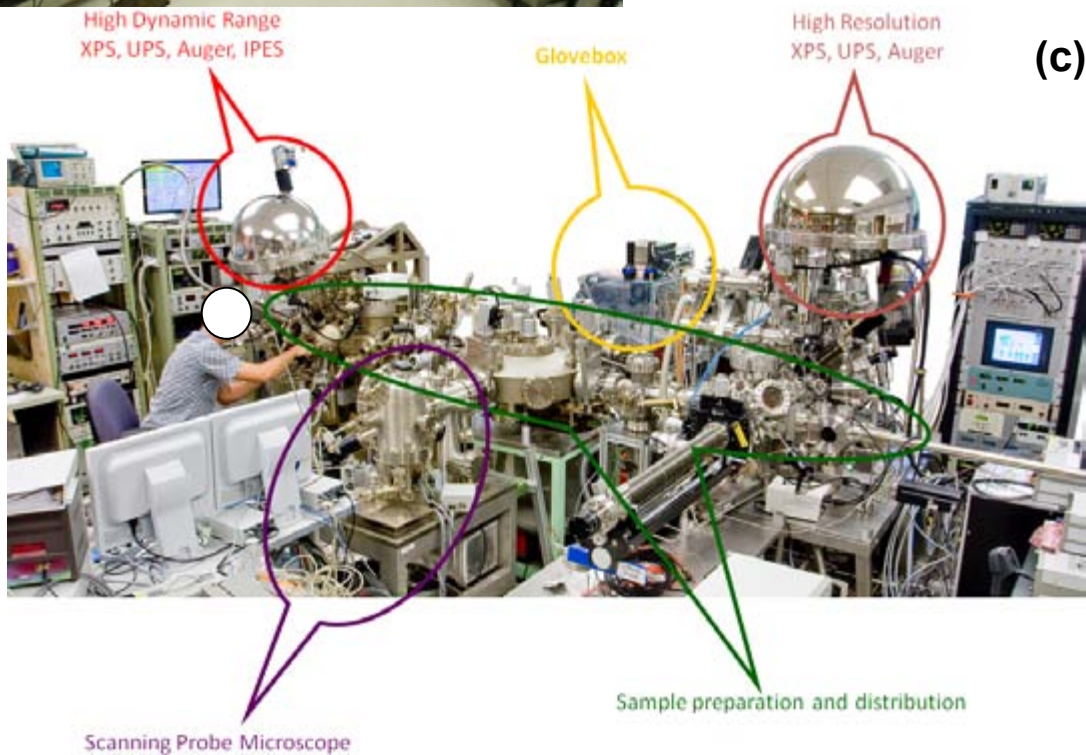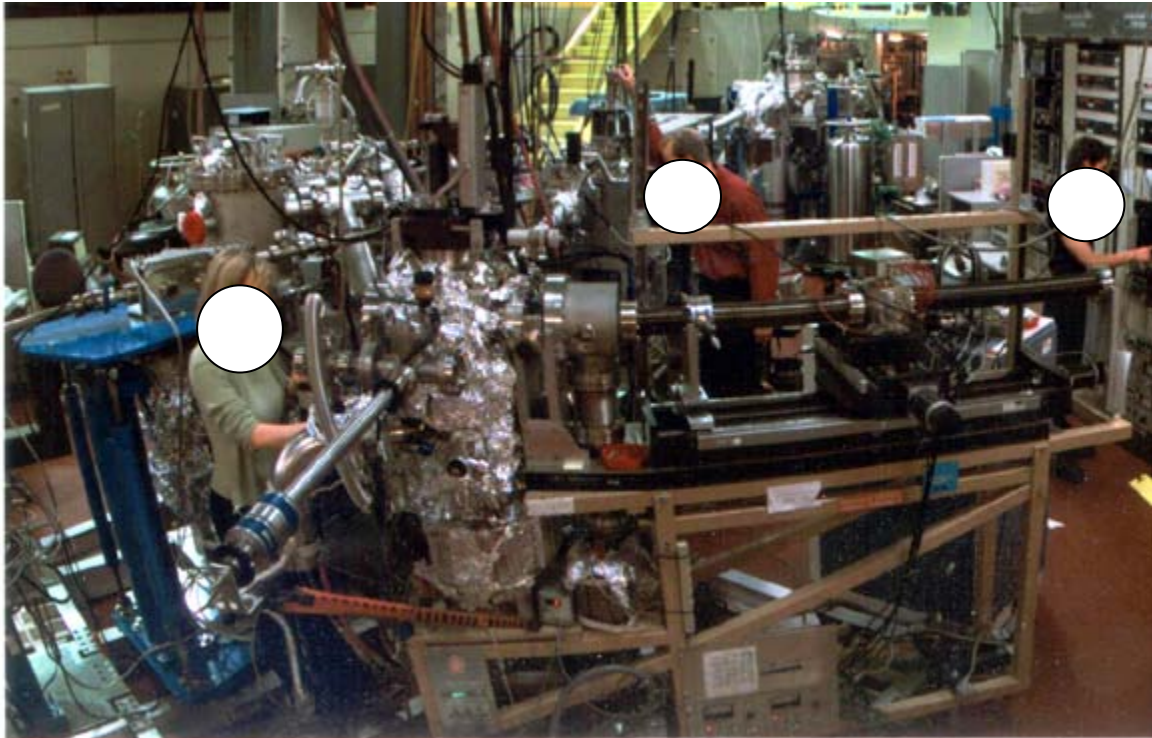
Fig. 3 *Beamline 8.0 (with SXF spectrometer in the front) at the Advanced Light Source (Lawrence Berkeley National Laboratory).*
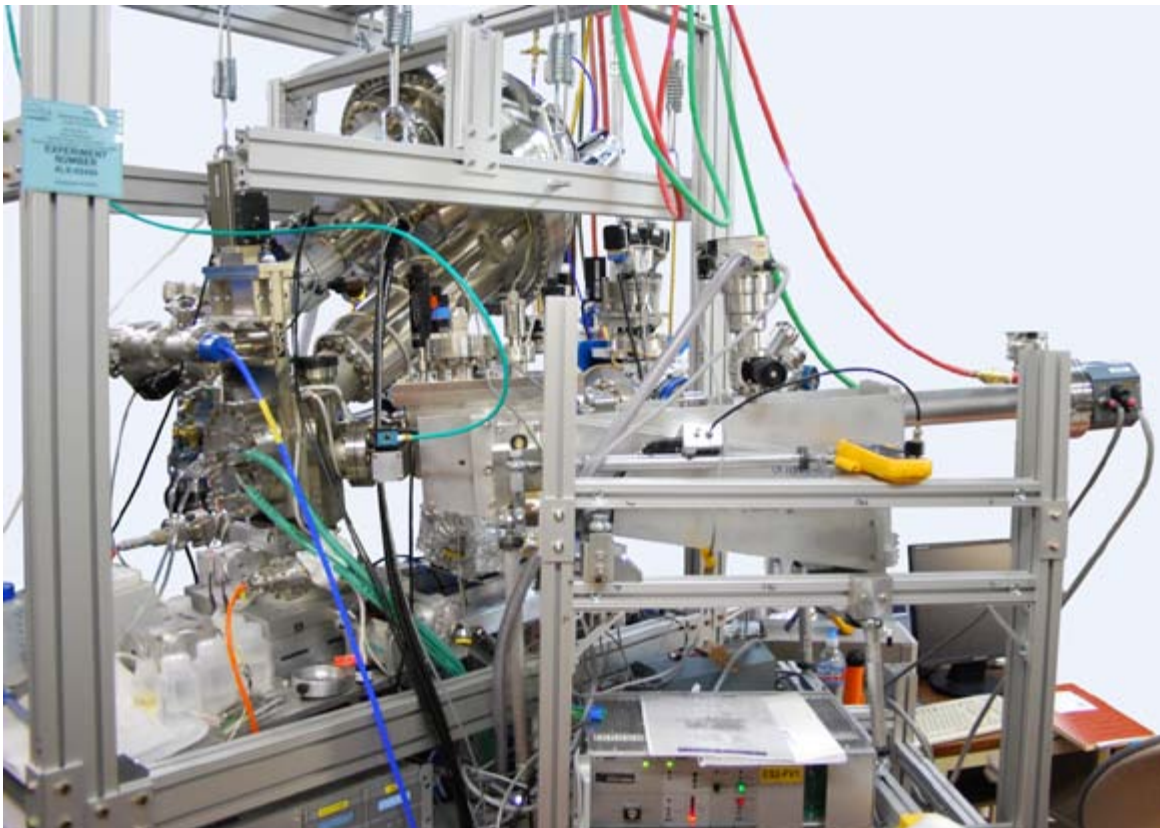
Fig. 4 *SALSA endstation at Beamline 8.0 of the ALS.*

3. Experimental Results

In the following, we will present some selected results of our work within the TFPPP program. First, we will report on our studies on laboratory-manufactured chalcopyrite-based thin film solar cell absorbers (A1-A5), then some results of our investigations on CdS/CdTe structures will be presented (B1, B2), and finally we will exemplary demonstrate how our spectroscopic methods can also help in the development of industrial-grade mass-produced Cu(In,Ga)Se$_2$ absorbers (C1).

A1. Chemical and electronic structure of 20.0% efficient Cu(In,Ga)(S,Se)$_2$ thin film solar cell absorbers
[Collaboration with I. Repins, M.A. Contreras, and R. Noufi, National Renewable Energy Laboratory, NREL]

In February 2008, the NREL group announced a new world record efficiency (20.0%, [1,2]) for Cu(In,Ga)Se$_2$ "CIGSe" – based thin-film solar cells. This recent efficiency gain (compared to the former world record - 19.5% [3]), is believed to be caused by a small – but apparently significant – change in the three-stage process [1]. In comparison to the deposition process used earlier, the difference resulting in the recent world record CIGSe absorber was a termination of the third (and thus last) stage without Ga and hence is considered to be "In-terminated" [1].
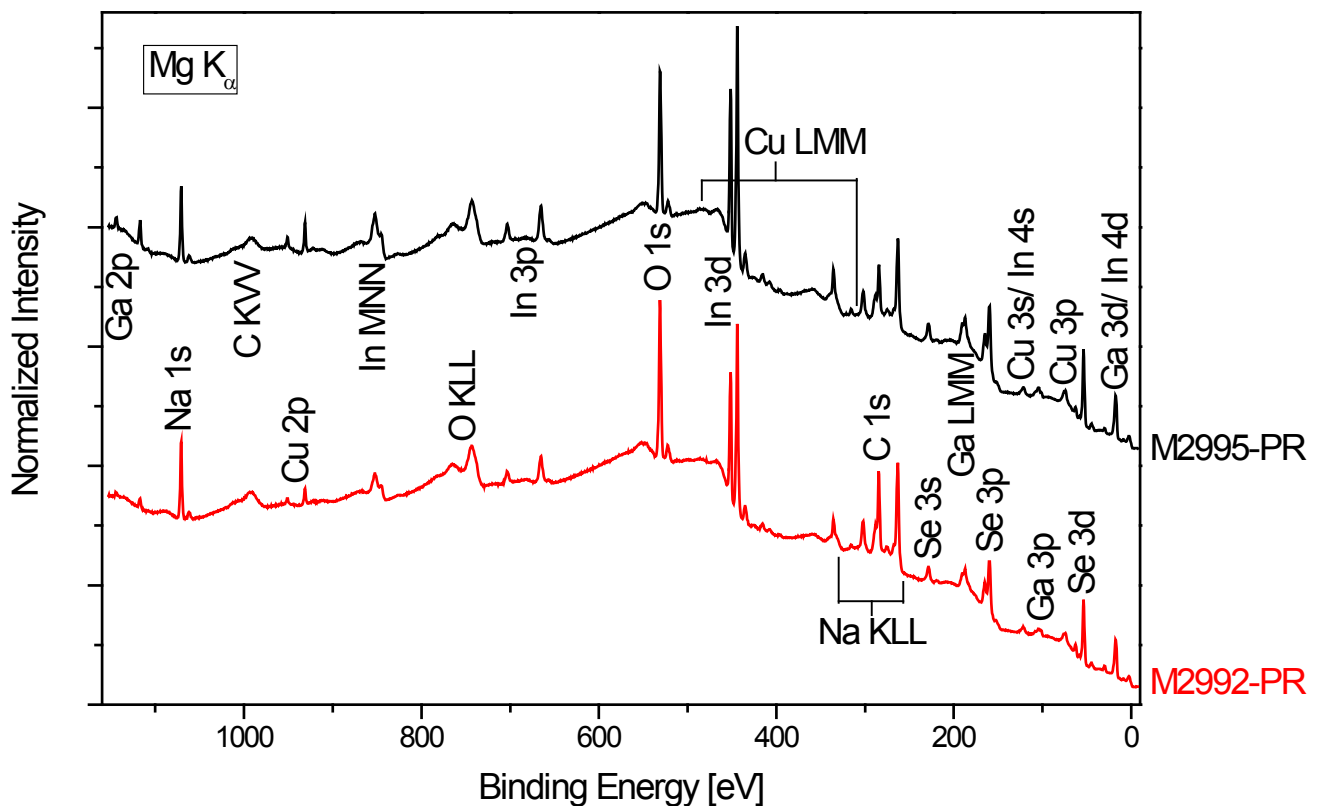
Fig. 5 *XPS survey spectra of the investigated CIGSe samples (as-received).*
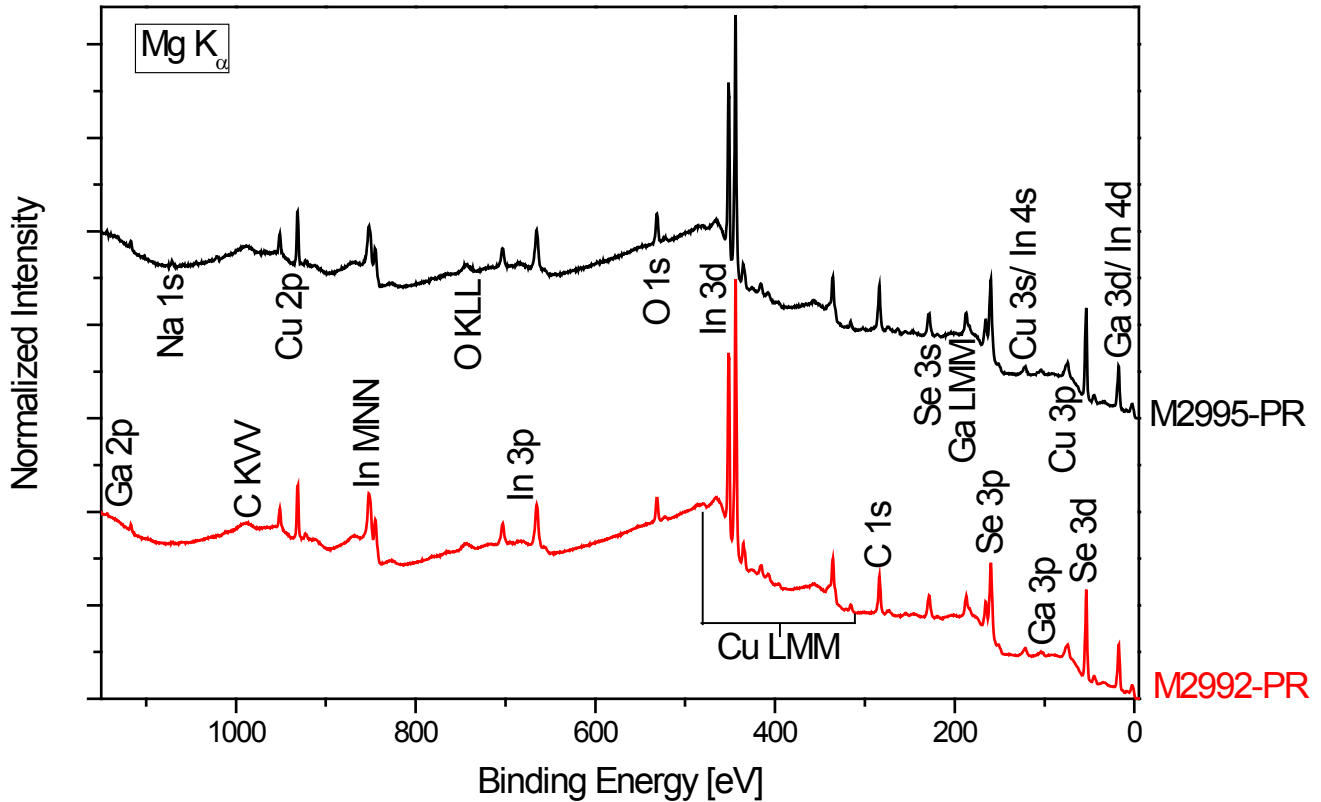
Fig. 6 *XPS survey spectra of the investigated CIGSe samples (after NH₃-dip).*

In order to shed light on the expected different chemical surface structure, we investigated a sample from the world record absorber batch (M2992) by XPS. As already mentioned this technique is very surface sensitive (information depth a few nm) and thus well suited to address questions of surface termination. In addition, we also characterized a CIGSe absorber (M2995) deliberately terminated with Ga for comparison.

Fig. 5 shows the XPS survey scans of the investigated CIGSe samples. As indicated by the high-intensity O-related XPS (O 1s) and XAES (O KLL) features, the surface of both samples is significantly oxidized. Corresponding detail spectra of photoemission and Auger features show that especially In and Ga are oxidized. The surfaces also show large amounts of Na and C. The C 1s photoemission line is composed of two pronounced contributions, of which the high-binding energy feature at approx. 289.6 eV is ascribed to carbonate. This interpretation also agrees with the line position of the O1s XPS peak. The position of the Na 1s photoemission line together with the modified Auger parameter of Na (Na 1s + Na KLL) furthermore suggests the formation of $NaCO_3$ at the sample surfaces. This pronounced sample surface contamination/oxidation can be explained by the extended storage of the samples in a desiccator and occasional exposure to air during different preceding characterization campaigns.

In the survey spectra in Fig. 5, we also observe a lower intensity of the Ga XPS and Auger features for the "In-terminated" sample (M2992) compared to the "Ga-terminated" sample (M2995). This could indeed be the first indication for the expected different Ga/In surface ratio for the two samples. Note that, however, the higher degree of surface contamination for the "In-terminated" sample (as evident

from the larger Na 1s, O 1s, and C 1s peaks) also leads to lower intensities of the corresponding In-related peaks. Since the emission of the Ga and In lines are governed by different attenuation lengths, a reliable quantitative analysis would require a detailed model of the nature, thickness, and morphology of the contamination layer, which is not available.

Usually, our group uses a mild (50 eV Ar$^+$) ion treatment to clean the samples we are investigating. This ion energy is chosen since it is below the sputter threshold for chalcopyrites, leading primarily to ion-stimulated desorption of adsorbates and minimizing potential damage to the actual surface. In the present case, however, the surface contamination/oxidation was very pronounced, and thus we decided to clean the samples chemically by means of a short (2 min) dip in aqueous ammonia (at room temperature) performed in our N$_2$-filled glovebox. The corresponding XPS survey spectra are shown in Fig. 6.

Compared to the XPS survey spectra in Fig. 5, the spectra in Fig. 6 show that the intensity of the Na-, O-, and C-related features is significantly reduced. Correspondingly, the Cu and In photoemission and Auger feature detail spectra do not show any indications for the presence of oxides at the sample surface anymore. Hence, as expected, the NH$_3$ dip cleaned the surface of the investigated CIGSe samples (note that the residual oxygen signal is ascribed to residue from the aqueous solution dip).

To minimize the impact of the residual surface contamination for the quantitative analysis of the surface composition, we have analyzed only photoemission lines in the low binding energy (E$_B$) region. Low E$_B$ photoelectrons correspond to high kinetic energy photoelectrons, which exhibit lower surface sensitivity (and susceptibility to surface contamination). Furthermore, the analyzed photoemission lines have kinetic energies within range of each other, which allows us to neglect the energy-dependence of inelastic mean free path of electrons and the spectrometer transmission function.

Fig. 7 shows the region of the low binding energy photoemission lines of the investigated In- (M2992, red) and Ga- (M2995, black) terminated CIGSe absorbers, respectively. For normalization of the two spectra, we derived the area intensity of the shown Cu, In, Ga, and Se core levels, weighted them with the respective photoionization cross sections [4], and summed them to give the overall spectral weight. Then, a normalization factor was chosen such that the normalized overall spectral weight for both spectra was equal.

At first sight, the spectra look very similar to each other -- they both show all expected Cu, In, Ga, and Se photoemission lines. However, close inspection of the Se 3d and Ga 3d/In 4d regions reveals small, but significant differences in the respective line intensities. As confirmed by the difference spectrum ([(a) – (b) = M2992 – M2995]; bottom spectrum in Fig. 7), the In-terminated absorber shows more intensity in the spectral region of the Se 3d and Ga 3d/In 4d XPS peaks. Due to the overlap of the Ga 3d and In 4d photoemission lines, it is not trivial to ascribe the higher overall intensity of the superimposed XPS peaks to a higher/lower Ga or In surface content. In order to address this situation, the Ga 3d and In 4d contribution to the Ga 3d/In 4d line was determined by a simultaneous fit of the corresponding spectral region for both samples. The inset in Fig. 7 shows the magnified region of the Ga 3d/In 4d XPS peaks along with the fitted Ga 3d and In 4d contributions for the spectra at 18 eV. The fit agrees well with the energetic position of the In 4d contribution. Close inspection of the difference spectrum also

shows that the position of the minimum (around 20 eV) is in accordance with that of the Ga 3d contribution. Hence, the In-terminated sample has a higher In content (by 7 ± 1 %) and the Ga-terminated sample a higher Ga content (by 9 ± 1 %) at the surface (as expected).
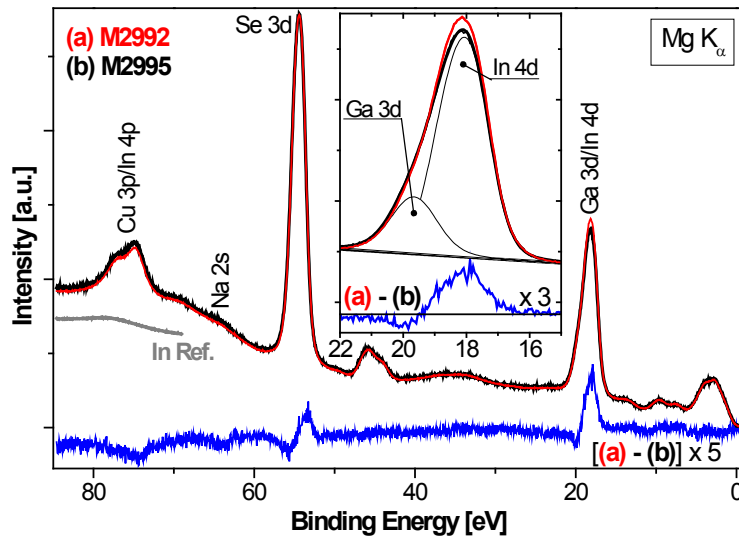
Fig. 7 *Region of the low binding energy photoemission lines of the investigated In- (M2992, red spectrum) and Ga- (M2995, black spectrum) "terminated" CIGSe absorbers. The magnified difference spectrum ([(a) – (b) = M2992 – M2995; blue spectrum] as well as the (scaled) In 4p spectrum of an In metal reference (gray spectrum) are also shown. The inset shows the magnified region of the Ga 3d/In 4d XPS peaks for both samples, together with the fitted Ga 3d and In 4d contribution for sample M2995. The computed difference spectrum is again shown for comparison.*

Taking the photoionization cross sections [4] into account, one can determine that the (In+Ga) surface content of sample M2992 is (2 ± 1) % higher than that of M2995. In addition, one can compute the Ga/(In+Ga) ratio of sample M2992 and M2995 are 0.29 and 0.32 (± 0.02), respectively (note that these values are in good agreement with the surface composition of the pristine samples reported in Ref. 1).

Contrary to the intensity increase of the spectral Ga 3d/In 4d region observed for the In-terminated sample, a decrease in intensity is observed for the Cu 3p/In 4p region (as best seen in the difference spectrum in Fig. 7). This suggests that the Cu surface content for the In-terminated sample is lower. In order to estimate the impact on the signal intensity in the Cu 3p/In 4p region caused by the observed In 4d variations, the In 4p photoemission line of an In metal reference (scaled according to the In 4d signal intensity of sample M2995) is shown in Fig. 7 for comparison. Apparently, the small change observed in the In surface content would have only a minor (*i.e.*, negligible) influence on the overall intensity in the spectral region of the Cu 3p/In 4p photoemission lines.

As additional features in the difference spectrum in Fig. 7 one can observe a local minimum and maximum at around 55 eV and a small dip at 64 eV. The latter feature is in the spectral region of the Na 2s photoemission line. This can be interpreted as a slightly higher Na surface content of sample M2995 sample compared to sample M2992. Since no pronounced Na 2s photoemission line can be observed, the Na concentration is close to the XPS the detection limit. Note that the photoionization cross section [4] of the accompanying Na 2p line (which one would expect at 31 eV) is less than that of the Na 2s line at

this excitation energy, and hence the related Na 2p difference feature is not visible due to an insufficient signal-to-noise ratio of the measured XPS spectra. The feature in the vicinity of the Se 3d XPS peak (around 55 eV), can be explained by a slight shift of the M2992 Se 3d photoemission line to lower binding energies.

The increase of the (Ga+In) and decrease in Cu surface content (at a similar Se surface content) for the In-terminated sample can also be interpreted as a more pronounced Cu deficiency for the In-terminated sample (note that both samples are Cu deficient compared to the stoichiometric Cu:(In+Ga):Se = 1:1:2 bulk composition). This is in good agreement with earlier publications, which show a Cu-poor surface composition for high-efficiency chalcopyrite absorbers [5-7].

In order to investigate the influence of different absorber terminations on the electronic surface structure, corresponding UPS and IPES measurements were performed. The recorded UPS (IPES) spectra of sample M2992 (in red) and M2995 (in black) are shown on the left (right) side of Fig. 8 on a common energy scale relative to the Fermi energy (E_F). A close look at the valence band (VB) region reveals that the UPS spectrum of the Ga-terminated sample M2995 has more intensity in the spectral region with contributions from Cu 3d-derived states (approx. 3 eV below E_F). This observation agrees with the earlier interpretation that the surface of the In-terminated sample is more Cu deficient. However, the position of the valence band maximum (VBM; defined by the leading edge of the UPS spectra) does not seem to be influenced by the changes in the surface stoichiometry, as best seen in the corresponding region shown in the inset of Fig. 8. The respective linear approximation [shown for the UPS spectrum of sample M2992; Fig. 8 (inset)] determines the VBM for both samples to be − 0.75 ± 0.10 eV. The spectral conduction band (CB) region of both samples appears very similar, but the IPES spectrum (and hence the respective conduction band maximum [CBM]) of sample M2992 is clearly shifted upward when compared to M2995 [ΔCBM = (0.20 ± 0.05) eV]. As apparent from the inset of Fig. 8, the leading edge of the IPES spectra (of as-introduced samples) is not as clearly defined (linear) as the respective UPS spectra or as IPES spectra of samples cleaned by mild Ar^{+} sputtering [6], leading to an increased uncertainty for the determination of the *absolute* CBM position. The linear approximation shown for the IPES spectrum of the In-terminated sample (Fig. 8, inset) results in a CBM estimate of (0.8 ± 0.3) eV above E_F, and the CBM is determined as (0.6 ± 0.3) eV for the Ga-terminated sample. Together with the determined VBM positions, the corresponding electronic surface band gaps (E_g^{Surf}) are [1.55 ± 0.3] eV and [1.35 ± 0.3] eV for the In- and Ga-terminated samples, respectively. These values are in good agreement with previously published surface band gaps for CIGSe absorbers [6,7]. However, the estimated E_g^{Surf} values are higher than the expected bulk band gap (~1.17 eV according to the quantum efficiency measurement of M2992 shown in Ref. 1) and the expected "theoretical" band gap [8] based on the here-determined surface Ga/(In+Ga) ratio (1.17 and 1.19 eV for sample M2992 and M2995, respectively). Our E_g^{Surf} finding is consistent with a Cu-deficient surface (found for both samples). Note that the observed higher Ga surface content of sample M2995 does not result in a larger E_g^{Surf} value (compared to M2992). Apparently, the less pronounced Cu deficiency (leading to a decrease in the band gap) counteracts the (expected) band gap increase with Ga content.
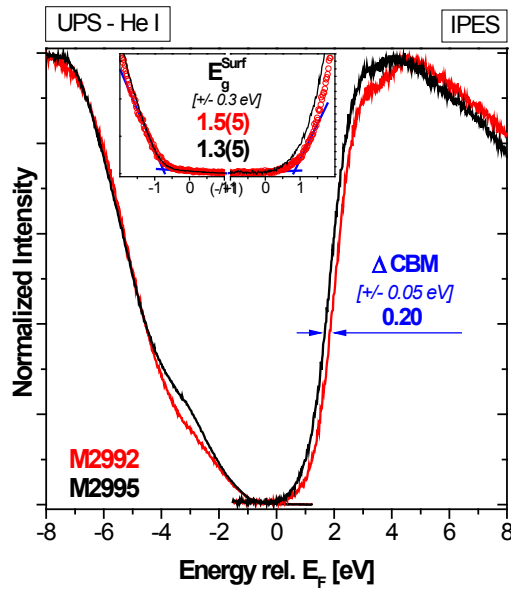
Fig. 8 *UPS (IPES) spectra of sample M2992 (red) and M2995 (black) are shown on the left (right) side on a common energy scale relative to the Fermi energy E_F. The inset shows the magnified region of the edge onsets. The linear approximation of the leading edges to derive the VBM and CBM is shown for sample M2992.*

The different solar cell performance of devices made from M2992 or M2995 absorbers is inferred from the observed different chemical and electronic surface structure. The larger E_g^{Surf} of the In-terminated absorber will have an impact on the interface formation with the CdS buffer layer. In order to address this question, a detailed analysis of the interface formation between the buffer layer and its respective absorber using XPS, UPS, and IPES is currently under way.

In summary, we have investigated the chemical and electronic surface structure of (world-record) CIGSe absorbers stemming from deposition processes with different growth termination. As expected, the In (Ga) "terminated" sample has a higher In (Ga) surface content. Furthermore, the surface of the In-terminated absorber is also (comparatively) Cu poor, which was interpreted as an increased Cu deficiency for the In-terminated sample. The surface band gap of the In terminated sample was found to be larger than that of the Ga terminated sample, indicating that the degree of Cu deficiency has a more pronounced impact on the surface band gap than the Ga/(In+Ga) ratio at the surface. Future experiments will clarify if these findings provide an explanation to the origin of higher solar cell device efficiencies in In-terminated CIGSe (as opposed to Ga-terminated) absorbers.

A2. The chemical and electronic structure of the CdS/Cu(In,Ga)Se$_2$ interface
[Collaboration with M.A. Contreras and R. Noufi, National Renewable Energy Laboratory, NREL]

In order to investigate the chemical and electronic structure of the CdS/CIGSe interface (note that CdS is the conventional junction partner of the CIGSe absorber in chalcopyrite-based thin film solar cells), we investigated a set of CdS/CIGSe samples from NREL. For those samples the CdS layer thickness was varied by means of taking the samples out of the chemical deposition bath after different times (0 - 16 min). See Table I for a complete list. All samples were characterized by XPS, UPS, IPES, and XES.

First, we will focus on our XES results. Fig. 9 shows the respective XES spectra of the Cd $M_{4,5}$ and In $M_{4,5}$ emission region on a linear (left) and logarithmic scale (right). Already after a deposition time of 1 min (and above), a Cd $M_{4,5}$ emission can be clearly identified (in particular on the logarithmic scale), which steadily increases with increasing deposition time. Consequently, the In $M_{4,5}$ emission intensity from the CIGSe substrate decreases due to the attenuation by the increasingly thick CdS layer. Close inspection of the data shows that the In $M_{4,5}$ emission is small, but still visible after a deposition time of 16 min. In order to quantify the thickness of the CdS layer using the XES data, we compared the CdS/CIGSe data with (reference) spectra of a thick CdS layer (not shown) and of the uncovered CIGSe substrate (bottom spectrum in Fig. 9). All measured spectra were described (in terms of a χ^2 fit) as a sum of the (weighted) reference CdS and substrate spectra:

$$sample = a \cdot CdS_{reference} + b \cdot substrate \quad (1)$$

To derive the thickness of the CBD-CdS layer deposited on CIGSe, we can use both, the attenuation of the In $M_{4,5}$ signal as well as the increase of the Cd $M_{4,5}$ intensity independently. If a homogeneous cover layer of thickness x attenuates the emission from the substrate, then the attenuated substrate emission intensity $I^{sub}(x)$ can be written as

$$I^{sub}(x) = I^{sub}_{ref} \cdot e^{-\frac{x}{\lambda*}} \quad (2).$$
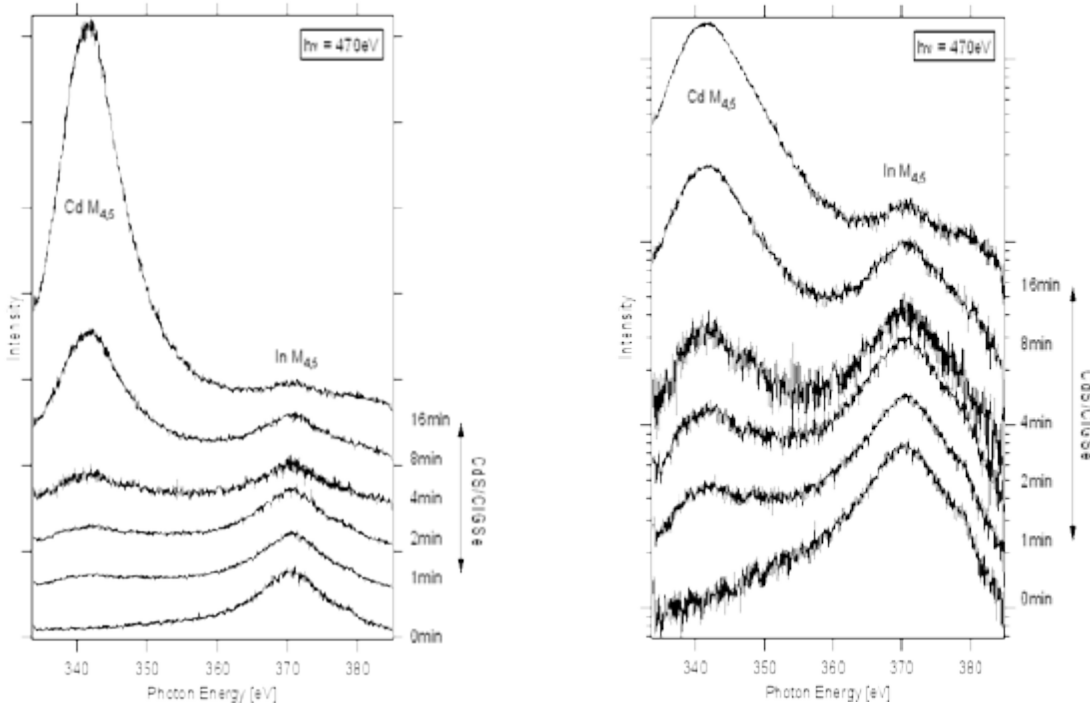
Fig. 9 *Cd $M_{4,5}$ and In $M_{4,5}$ X-ray emission spectroscopy of the investigated set of CdS/CIGSe samples on a linear (left) and logarithmic scale (right).*

Similarly, the intensity of the emission from the cover layer $I^{cov}(x)$ can be written as

$$I^{cov}(x) = I^{cov}_{ref}\left(1 - e^{-\frac{x}{\lambda*}}\right) \quad (3).$$

I^{sub}_{ref} and I^{cov}_{ref} denote the reference emission intensity of an uncovered substrate and of a cover layer of sufficient thickness, respectively ("sufficient" corresponds to a material thickness that results in a saturated emission intensity). Furthermore,

$$\frac{1}{\lambda*} = \left(\frac{1}{\lambda_{exc} \cdot \sin\alpha}\right) + \left(\frac{1}{\lambda_{em} \cdot \sin\beta}\right) \quad (4),$$

Table I
List of the investigated samples with corresponding CdS buffer deposition time.

Sample	CdS Deposition Time
C2106-11	0 min, bare absorber
C2106-21	1 min
C2106-12	2 min
C2106-22	4 min
C2106-18	8 min
C2106-23	(2 × 8) 16 min

where λ_{exc} and λ_{em} are the attenuation lengths in the cover layer for the excitation and emission energy, respectively. α and β are the angles of excitation and emission relative to the sample surface, respectively (in our case $\alpha = \beta = 45°$). In order to obtain the cover layer thickness x, we used the above-determined weighting factors $a = I^{cov}(x) : I^{cov}_{ref}$ and $b = I^{sub}(x) : I^{sub}_{ref}$ (see Eq. 1). The attenuation lengths associated with the Cd $M_{4,5}$ and In $M_{4,5}$ emission energies, the excitation energy, and the specific overlayer material (here: CdS) are listed in Table II. Assuming that the CdS layer homogeneously covers the substrate (as it can be expected if prepared by a wet-chemical deposition method such as CBD), the layer thicknesses on CIGSe were determined and are shown in Fig. 10 as a function of the deposition time. The given error is assumed to be dominated by the uncertainty in comparing absolute XES intensities due to sample (mis)alignment and is estimated to be 10% for the above-mentioned intensity ratios. For deposition times of 2 min and above, the values determined using the attenuation of the In $M_{4,5}$ CIS emission are (within the error bars) quite similar to those calculated from the increasing Cd

14
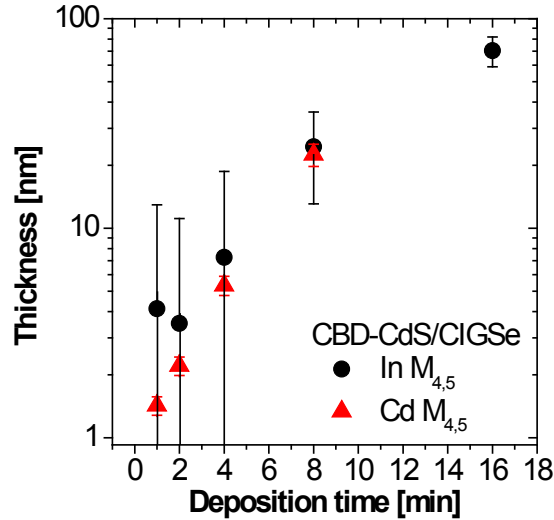
Fig. 10 *CdS layer thickness determined from the attenuation of the In $M_{4,5}$ emission of the substrate or from the increase of the Cd $M_{4,5}$ emission from the cover layer, respectively.*

$M_{4,5}$ cover layer emission intensity. Thus, both approaches (Eq. (2) and (3)) give consistent numbers. For thin cover layers the thickness determination based on the Cd $M_{4,5}$ emission intensity is more reliable as indicated by the smaller error bars. The thickness of the CBD-CdS layer after a deposition time of 16 min (which corresponds to the standard CdS buffer) on CIGSe is determined to be (70 ± 11) nm.

Table II
X-ray attenuation lengths in CdS (taken from [9]).

λ_{CdS} Cd $M_{4,5}$ emission (341.3 eV)	λ_{CdS} In $M_{4,5}$ emission (370.4 eV)	λ_{CdS} excitation (470.0 eV)
189 nm	216 nm	128 nm

S $L_{2,3}$ spectra of the investigated samples and of a CdS reference were also recorded. They are shown in Fig. 11 again on a linear (left) and a logarithmic scale (right). The main peak of the CdS reference spectrum at 147.3 eV (which is actually a doublet indicated by the clearly visible shoulder at 149 eV) is due to S 3s electrons decaying into S $2p_{1/2}$ and S $2p_{3/2}$ core holes. In addition, the two peaks at 150.5 eV and 151.8 eV correspond to Cd 4d electrons decaying into the S $2p_{1/2}$ and S $2p_{3/2}$ core holes, respectively. They thus directly indicate sulfur atoms bound to Cd. Furthermore, we observe the upper valence band of CdS at about 156 eV. Comparing the spectra of the CdS/CIGSe samples with that of the CdS reference, it is obvious that they also show the typical features of a CdS S $L_{2,3}$ spectrum, especially when compared on logarithmic scale. As expected, this becomes more distinct with increasing deposition time.
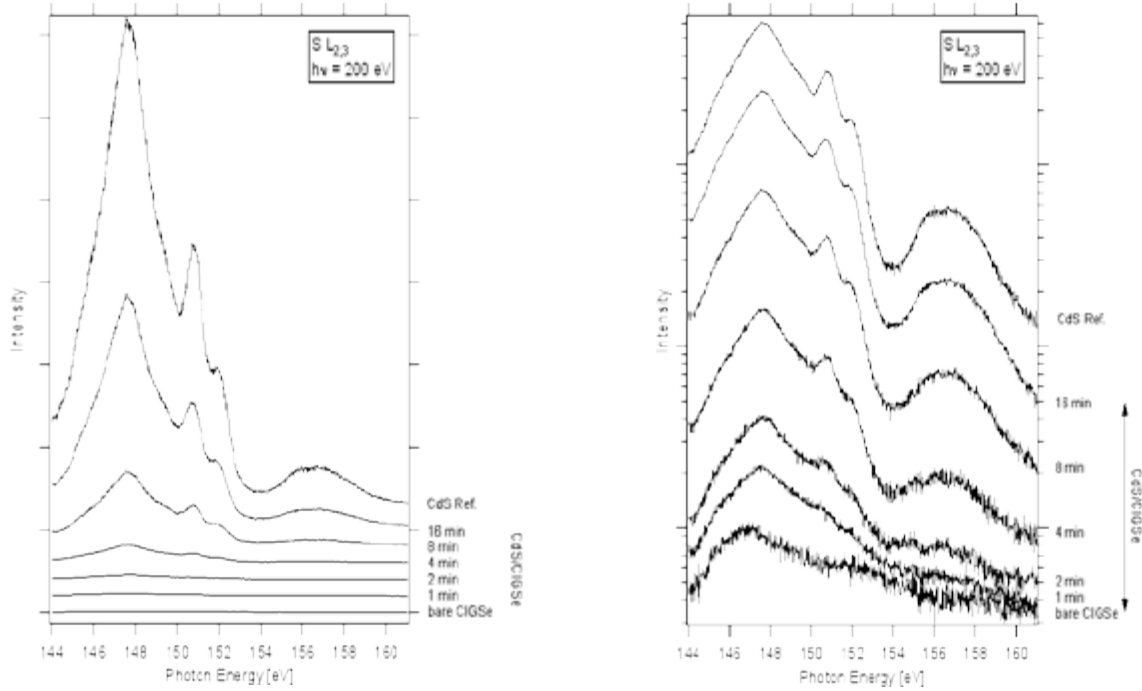
Fig. 11 *S L$_{2,3}$ emission of the investigated set of CdS/CIGSe samples on a linear (left) and logarithmic scale (right). For comparison also the spectrum of a CdS reference is shown.*
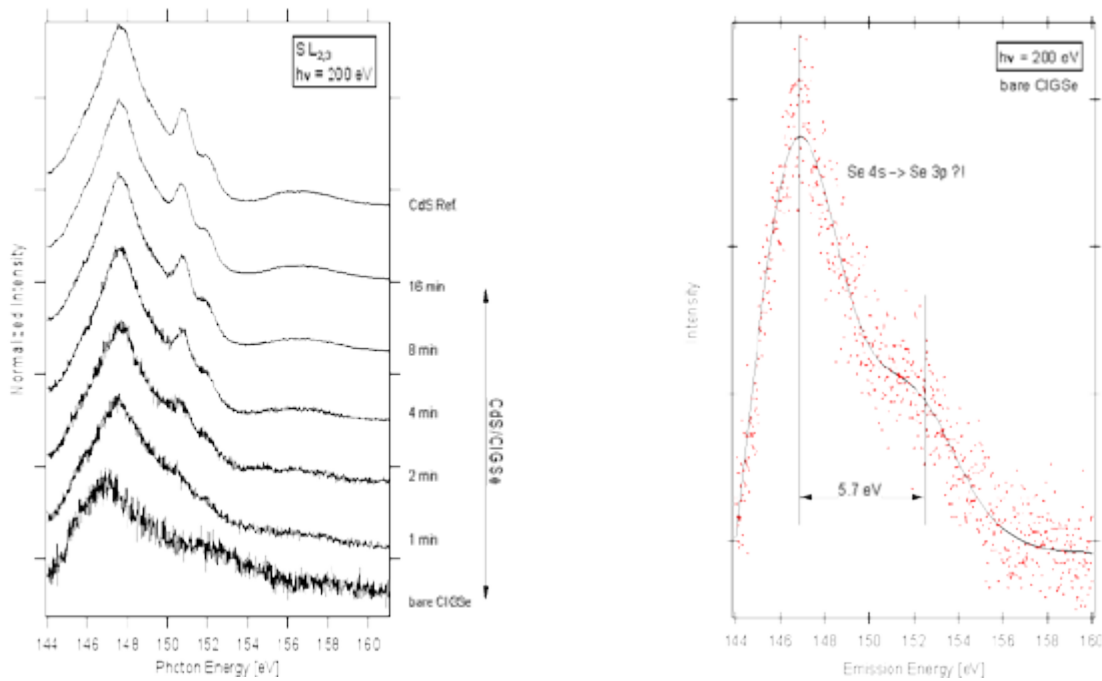
Fig. 12 *Normalized S L$_{2,3}$ emission of the investigated set of CdS/CIGSe samples (left). Magnified and smoothed presentation of the spectrum of the bare CIGSe sample (right): red dots: original data, black solid line: smoothed spectrum.*
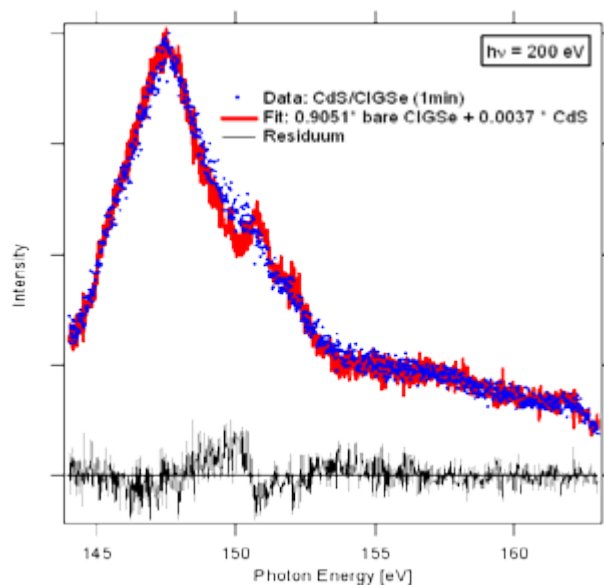
Fig. 13 *Comparison of the 'S L$_{2,3}$ spectrum' of the "1 min" CdS/CIGSe sample with a weighted superposition fit. In addition, also the residuum (difference between data and fit) is shown.*

In an earlier paper [10], the absence of the features indicating S-Cd bonds was indicative of intermixing processes at the CdS/CIGSe interface. For a detailed evaluation of whether such effects also play a role here, the new spectra are shown in Fig. 12, left, with normalization to their maximum. It can be observed that the spectrum of the bare (S-free!) CIGSe substrate shows different spectral features compared to the spectra of the S-containing samples. A magnified (smoothed) presentation of the CIGSe XES spectrum shown in Fig. 12 (right) reveals two spectral features, which are separated by 5.7 eV. Since the latter agrees well with the doublet separation of Se 3p$_{1/2}$ and Se 3p$_{3/2}$, the features can most likely be attributed to Se 4s electrons decaying into Se 3p$_{1/2}$ and Se 3p$_{3/2}$ core holes. Note that our group has (for the last ten years) repeatedly searched for such Se 3p emission peaks; only recently, a significant improvement of the XES spectrometer has made it possible to observe such very weak structures.

A similar analysis approach as used above (i.e., describing the CdS/CIGSe spectra as a sum of the weighted reference CdS- and CIGSe-spectra) was used to clarify whether the intensity ratio between the features directly indicating S-Cd bonds and the main S 3s peak changes with deposition time or whether the spectra of the CdS/CIGSe samples can be explained by a (weighted) superposition of CdS and bare CIGSe reference spectra. The exemplary comparison of the experimental data of the "1 min" sample with a respective fit is shown in Fig. 13. The fit agrees quite well with the experimental data except between 150 -153 eV (the spectral range of the features directly indicating S-Cd bonds). We thus conclude that the spectra taken for thin CdS films cannot be explained by a mere superposition of the Se substrate signal and the CdS reference. Nevertheless, in contrast to our earlier work, we find a clear Cd 4d signature (albeit smaller than for the CdS reference) even for the thinnest CdS film. Surface-sensitive XPS experiments in Fig. 16 additionally show that after 16 min deposition the Se 3d XPS signal vanishes, which is again in contrast to earlier experiments on CdS/CIGSe samples from a different source [10].
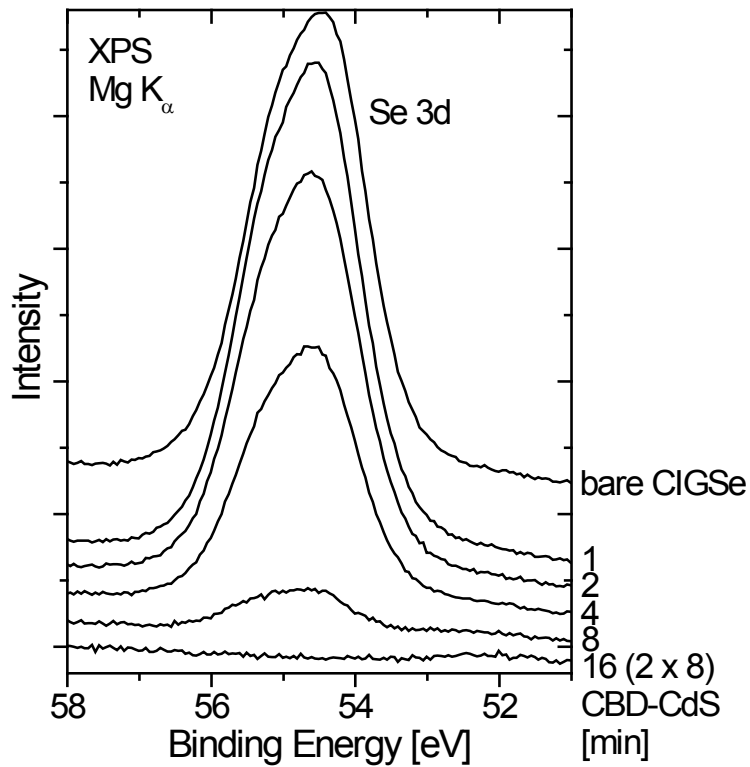
Fig. 14 *Se 3d XPS detail spectra of the CdS/CIGSe sample set.*
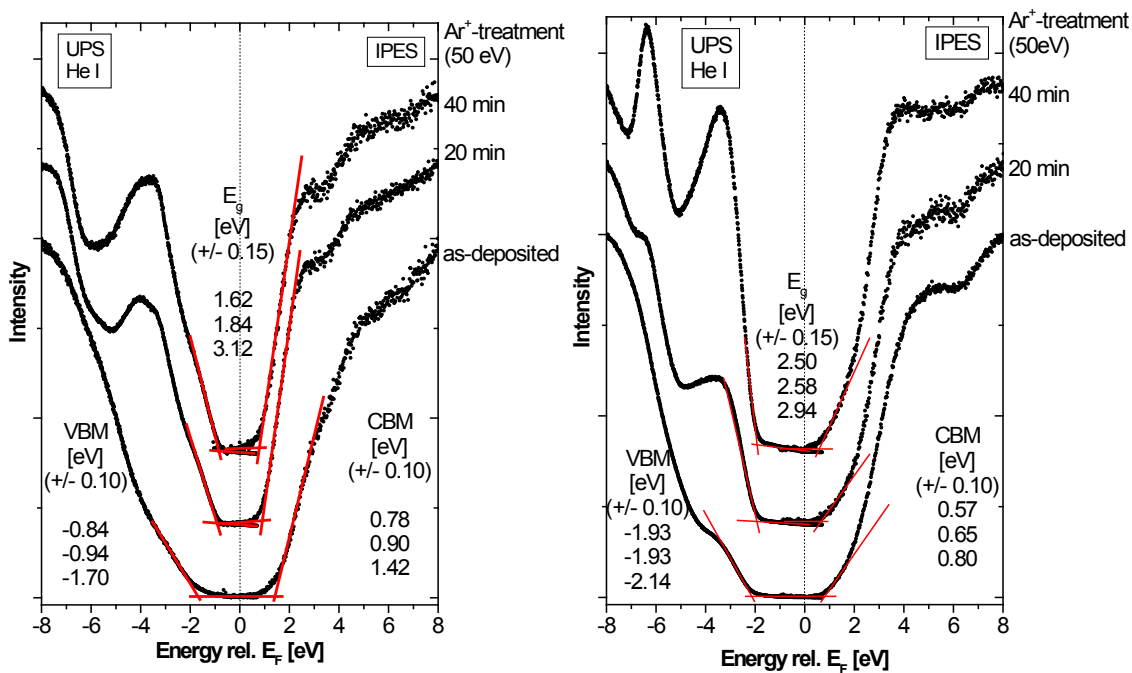
Fig. 15 *UPS and IPES spectra of absorber film (left) and the thick (16 min) CdS layer on CIGSe (right). To remove adsorbates from the surface both samples have been exposed to a mild Ar$^+$ ion treatment. The positions of the valence band maximum and conduction band minimum as derived by a linear extrapolation of the leading edges are given next to the spectra. The distance between valence band maximum and conduction band minimum gives the surface band gap, which is also listed.*

This can be interpreted in the following way: We do not find any evidence for a significant S/Se intermixing process. Nevertheless, the environment of the sulfur atoms at the growth start of the interface clearly deviates from a perfect CdS environment. Whether this is due to a less perfect crystalline structure (i.e., the formation of very small nm-scale nanoparticles [11]) or some sulfur diffusing into the CIGSe absorber cannot unambiguously be differentiated.

In the following our measurements with respect to the electronic interface structure are presented and discussed. For determining the band alignment at the interface, we have measured the valence and conduction band edges of the absorber film and the thick CdS film using UPS and IPES, as shown in Fig. 15. While samples were packed carefully, surface contaminations with C and O cannot be entirely prevented. These surface contaminations obscure the determination of the band edges, clearly seen by the attenuated valence band signal related to Cu 3d electrons for the CIGSe absorber film (bottom left spectrum in the left panel of Fig. 15). Only after mild Ar$^+$ ion treatment of the surface (50 eV ions at a sample current of approx. 100 nA), we are able to remove these contaminations without structural damage to the absorber surface. After about 40 min of ion treatment, no further changes in the spectra are observed, and we can derive a surface band gap for the CIGSe absorber film of 1.63 ($\pm$0.15) eV. This band gap is increased with respect to the optical bulk value (1.23 eV), which can be explained by the copper-poor stoichiometry of the sample that we derive from our XPS measurements.
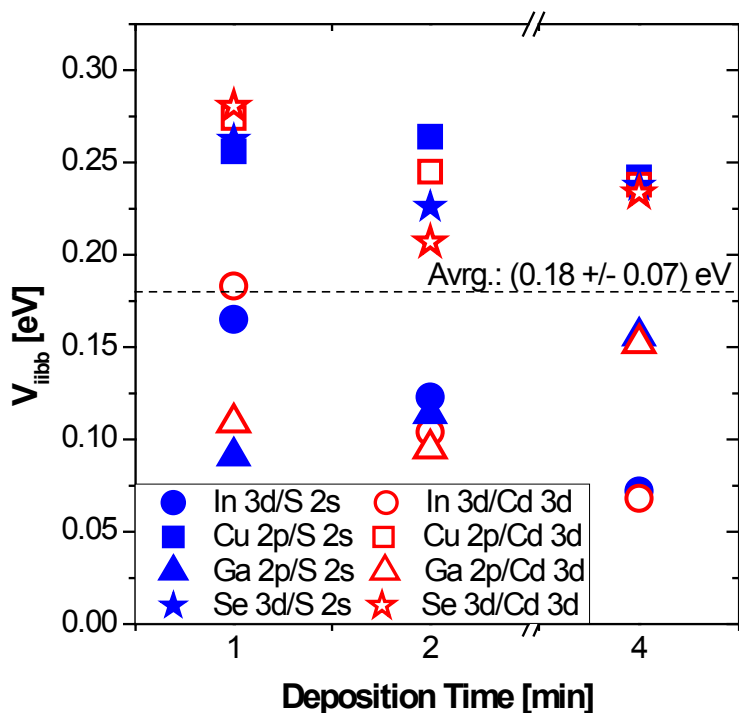
Fig. 16 *Values of the interface-induced band bending (iibb) as derived from monitoring the line shifts of different core levels.*

Similarly, the investigation of the CdS surface shows an increased surface band gap for the as-prepared surface. After cleaning with Ar$^+$ ions for 20 minutes the influence of the surface contaminations is largely removed, giving us a surface band gap of 2.50 ($\pm$0.15) eV, which agrees well with the (optically measured) bulk band gap of CdS.

The band alignment at the CdS/CIGSe interface is now determined in two steps. In the first (approximate) step, we compare the band edge positions of the CIGSe absorber with those of the thick CdS/CIGSe film which are given in Fig. 15. This first approximation indicates a small cliff of 0.21 eV.

This value has now to be refined in the second step to account for changes in band bending of the absorber occurring when the interface to the CdS buffer layer is formed. This can be achieved by following the shifts of XPS core level positions of the absorber and the CdS buffer layer using the thin CdS/CIGSe samples (1, 2, and 4 min) where both lines from the CIGSe absorber and from the CdS buffer layer are visible. To minimize effects due to chemical shifts caused by bonding at the interface as well as possible intermixing of the layers, we have used different combinations of core levels of the CIGSe absorber and the CdS buffer layer as shown in Fig. 16. In total we have derived 24 different values and get a mean value of 0.18 ($\pm$0.07) eV. Compared to earlier investigations of this interface with different CIGSSe absorbers [6,12,13], this is the largest interface-induced band bending we have found, indicating the presence of an interface dipole. Furthermore, the overall spread of the various V_{iibb} values is smaller than that of other CdS/CIGSe interfaces for which significant S/Se intermixing at the interface could be shown [10] (note that, as reported above we did not find an indication for S/Se intermixing in the case of the investigated NREL samples). These findings indicate a somewhat different chemical and electronic character of the CdS/CIGSe interface formation process at NREL compared to our previous work.
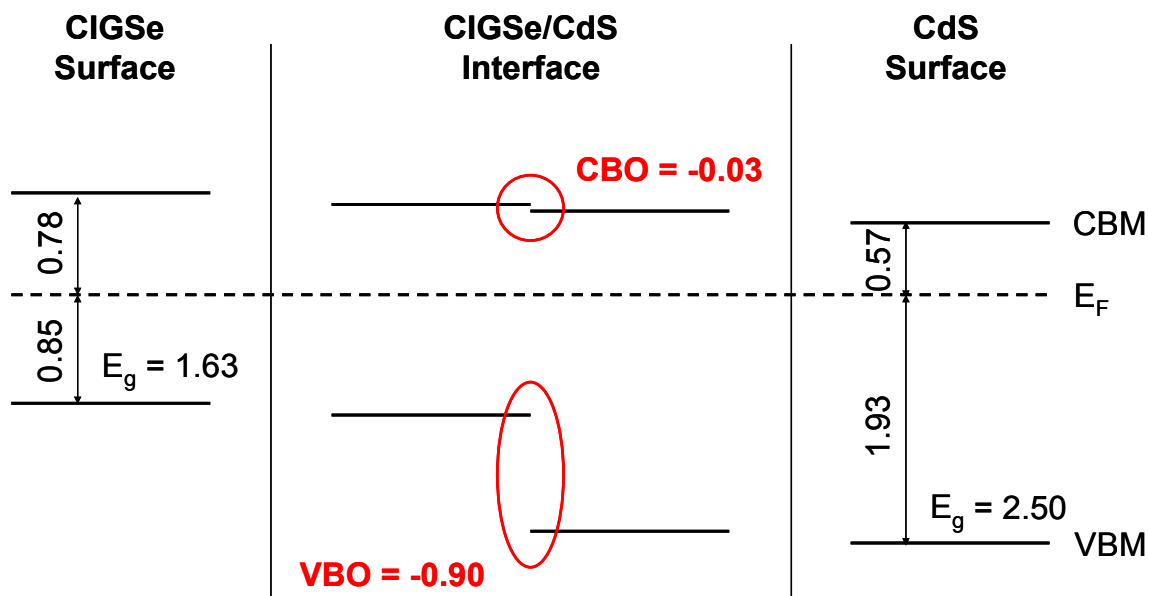
Fig. 17 *Schematic diagram of the band alignment at the CdS/CIGSe interface (all values are given in eV). The band extrema of the CIGSe and CdS surfaces (as determined by UPS and IPES) are shown on the left and right, respectively. The center shows the band alignment at the interface after taking the interface-induced band bending into account.*

We can now apply the correction for the interface-induced band bending to the conduction band minimum and valence band maximum values derived above to get the band alignment at the CdS/CIGSe interface. The results are shown in Fig. 17. We find a valence band offset of -0.90 (±0.15) eV and a flat conduction band alignment with an offset of -0.03 (±0.15) eV.

In summary, we have derived the electronic structure of the CdS/CIGSe interface in thin film solar cells prepared by NREL. The conduction band alignment at the CdS/CIGSe interface is flat, as expected for a high efficiency CIGSe solar cell. Furthermore, we find direct evidence for a strong interface dipole. Together with the previously reported lack of significant intermixing at the CdS/CIGSe interface, we thus find a modified electronic and chemical interface structure compared to previously studied (less efficient) devices from other manufacturers.

A3. Depth-dependent band gap in chalcopyrite thin-film solar cell absorbers

[Collaboration with the S. Nishiwaki and W. Shafarman, Institute of Energy Conversion, IEC, U Delaware]

This investigation is initially based on two kinds of samples: S-free CIGSe/Mo/glass and S-containing CIGSSe/Mo/glass test structures. The chalcopyrite absorber films (approx. 2 μm thick) were prepared using multi-source thermal co-evaporation without intentional composition gradients. The Mo-coated soda-lime glass substrate was held at 550°C during absorber formation (see Ref. 14 for more details).

The samples were investigated by different spectroscopic techniques in order of greatest surface sensitivity. The samples were first characterized by UPS and IPES, since these (electron-based) techniques are most surface sensitive among the applied spectroscopies and thus would be most influenced by any surface contamination. Next, the electronic structure of the surface-near bulk of the samples was investigated by XES/XAS at the ALS. For the transport to the ALS, the samples were again carefully packed and sealed in an inert atmosphere. Once at the ALS, the samples were mounted in and transferred through ambient air into the UHV analysis chamber of the SXF endstation (base pressure below $5 \cdot 10^{-8}$ mbar). Finally, the samples were transferred back to UNLV (in air) and optical reflection spectra of the CIGSe and CIGSSe samples were measured using a conventional UV-Vis-NIR spectrophotometer (Varian, Cary 5000).

The spectra recorded for the CIGSe and CIGSSe samples by the different spectroscopic techniques are shown in Fig. 18. The different spectra (optical reflection, left; XES/XAS, center; UPS/IPES, right) allow a determination/estimation of the E_g of the investigated samples with three different information depths, as will be described in the following. As shown in Fig. 18 (left), the optical reflection spectra exhibit pronounced interference patterns. These (Fabry-Perot) oscillations are caused by interference of light reflected at the absorber/air and absorber/substrate interfaces and thus depend on the thickness d of

the absorber and its absorption coefficient α. For photon energies higher than E_g, no oscillations are observed since the photons are completely absorbed in the CIGSe (CIGSSe) layer. In the spectral region with pronounced interferences the CIGSe (CIGSSe) absorber must consequently be transparent. Hence, in first approximation, the photon energy at which the oscillations in the reflection spectrum disappear corresponds to the E_g. To further refine this approach, we note that the E_g is actually shifted to lower energies since the absorption coefficient only gradually increases above E_g and since the thickness d of

$$2\alpha d = \ln\left[\frac{(R_{max} - R_{min})}{(R - R_{min})}\right] \qquad (5)$$

the absorber is sufficiently small that some light reflected at the absorber/substrate interface (although attenuated) will still be able to interfere with light reflected at the absorber/air interface. Thus, our approach to determine E_g from the "oscillation-free" reflectance R is as follows. We assume that the interferences oscillate around the "true" reflectance value and thus approximate R by the mean of the interference maxima and minima. Based on the respective envelopes of the extrema (fitted by 2nd order
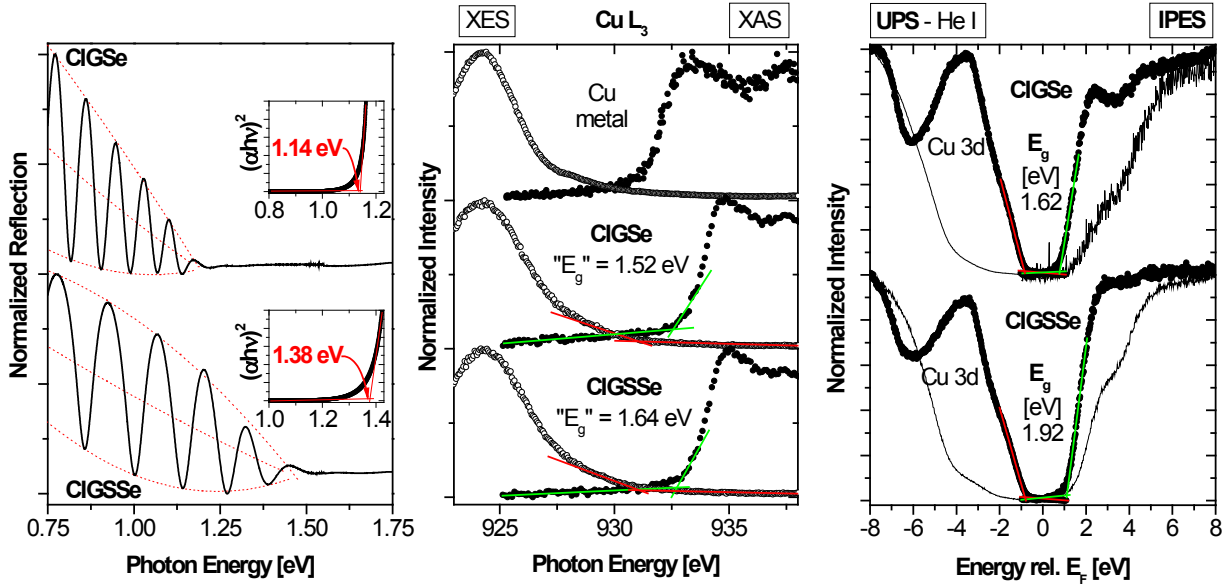
Fig. 18 Left: *Optical reflection spectra of the investigated CIGSe (top) and CIGSSe (bottom) sample. The respective envelopes of the interference extrema and the constructed mean values (red dotted lines) are also shown. Insets: Approximated absorption coefficient for the CIGSe (top) and CIGSSe (bottom) sample plotted as $(\alpha h\nu)^2$ vs. the photon energy $h\nu$. The given band gap energies have an error of ± 0.05 eV.*

Center: *Cu L_3 x-ray emission (XES, left) and absorption (XAS, right) spectra of the investigated CIGSe (middle spectra) and CIGSSe (bottom spectra) samples. For comparison, the spectra of metallic Cu (top) are also shown. The linear approximation of the leading edges for the determination of "E_g" (a lower bound for the true band gap value – see text) is indicated by the solid green and red lines. The given band gap energies "E_g" have an error of ± 0.20 eV.*

Right: *UV photoelectron spectroscopy (UPS, left) and inverse photoemission (IPES, right) measurements of the investigated CIGSe (top spectra) and CIGSSe (bottom spectra) samples. For each sample, two sets of spectra are shown, one for the as-introduced (thin solid lines) and one for the cleaned samples (dots). The linear approximation of the leading edges for the determination of E_g is indicated by the solid green and red lines. The given band gap energies E_g have an error of ± 0.15 eV.*

polynomials; see Fig. 18, left) the mean spectral characteristic of R can be constructed. The absorption coefficient was estimated by applying Eq. (5) [15], where R_{max} (R_{min}) is the maximal (minimal) reflectance in the considered spectral range (note that this approach gives reasonable results since the absolute value of α is not relevant for the estimation of E_g). Since it is well known that Cu chalcopyrites are direct semiconductors, the approximated absorption coefficient is plotted as $(\alpha h\nu)^2$ vs. the photon energy $h\nu$ to determine E_g (see insets in Fig. 18, left). We find a band gap energy of $[1.14 \ (1.38) \pm 0.05]$ eV for the CIGSe (CIGSSe) absorber.

Fig. 18 (center) shows the Cu L_3 XES and XAS spectra of the investigated CIGSe and CIGSSe samples. For comparison also the spectra of metallic Cu are shown. Since XES and XAS probe occupied and unoccupied states, respectively, the combination of both spectra gives information about E_g. However, the band gap values based on these measurements are approximate and represent a lower limit due to the potential existence of core exciton features in the XAS spectra. E_g was determined as the intersection of the baseline with a linear extrapolation of the leading XES and XAS edges. The E_g for the CIGSe (CIGSSe) absorber is found to be $[1.52 \ (1.64) \pm 0.20]$ eV.

Finally, the corresponding surface-sensitive UPS and IPES spectra of the investigated CIGSe and CIGSSe samples are shown in Fig. 18, right. For each sample, two sets of spectra are shown: One for the as-introduced and thus surface-contaminated sample and one after cleaning the sample surface by an ion-stimulated desorption process with 50 eV Ar^+ ions. Similar to the XES and XAS measurements, UPS and IPES give information about the occupied and unoccupied states, respectively. Hence, by combination of both techniques it is possible to measure the band gap at the *surface*. Again, linear extrapolation of the leading edges of the UPS and IPES spectra is used to determine the valence band maximum (VBM) and conduction band minimum (CBM), respectively, resulting in the surface band gap E_g = CBM - VBM. For the clean surface of the CIGSe (CIGSSe) absorber we find a band gap energy of [1.62 (1.92) ± 0.15] eV.

In order to understand the observed variations in E_g, the information depth of the different spectroscopic techniques has to be considered. Under the assumption that $\alpha \approx 10^4$ cm^{-1} for photon energies slightly above E_g (as reported for $CuInSe_2$ [16]) the information depth of the optical reflection measurement is $\approx$ 2000 nm, which is in the range of the thickness of the investigated CIGSe (CIGSSe) layers (note that for this and the following considerations the information depth is defined as the thickness from which 90% of the overall signal is collected). XAS (in total fluorescence yield mode) and XES have similar
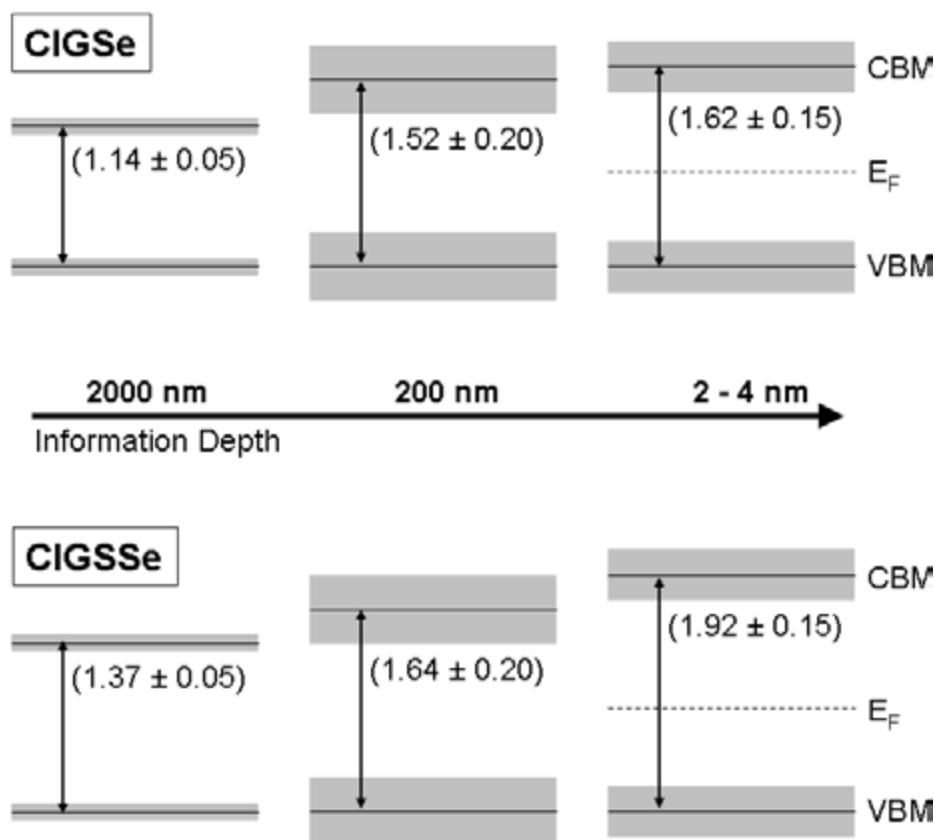
Fig. 19 *Schematic presentation of the determined band gap energies of the investigated CIGSe (top) and CIGSSe (bottom) samples using the three different spectroscopic approaches (optical reflection, left; x-ray emission and absorption, center; UV photoelectron spectroscopy and inverse photoemission, right). The respective information depths of the applied spectroscopies are also shown. The gray area represents the measurement error.*

information depths ($\approx$ 200 nm) (based on [9]). According to the "universal curve" [17], the inelastic mean free path (IMFP) of the detected photoelectrons for the UPS (He I) measurements of the investigated CIGSe (CIGSSe) samples is $\approx$ 10 Å, which results in an information depth of $\approx$ 2 nm. The information depth of our IPES measurements is approx. twice that of the UPS technique.

Fig. 19 shows a summary of our results. It shows a schematic presentation of the determined band gap energies of the investigated CIGSe (CIGSSe) sample using the three different spectroscopic approaches (optical reflection, left; XES/XAS, center; UPS/IPES, right) as a function of the information depth. For the investigated CIGSe (CIGSSe) samples we find an increasing band gap energy with decreasing information depth and, in particular, the formation of a surface region with significantly higher E_g. The smaller difference of the band gap energies determined by XES/XAS and UPS/IPES for the CIGSe sample compared to that for the CIGSSe sample suggests that the E_g-widened (i.e., Cu-poor) region is more pronounced for the CIGSe absorber.

Currently we are extending our experiments also to wide-gap chalcopyrites such as $CuInS_2$ and $CuGaSe_2$ in order to test the hypothesis that the E_g-widened surface region is less pronounced for absorbers with larger bulk band gaps. This might explain the lower performance of devices based on wide-gap chalcopyrite absorbers compared to the world record efficiencies reported for their low-gap counterparts.

In summary, we presented a detailed study that demonstrates how a combination of various spectroscopic techniques can be used to derive depth-dependent band gap information for compound semiconductors. We find that the band gap of $Cu(In,Ga)(S,Se)_2$ thin film solar cell absorbers varies greatly as a function of depth and that this variation is dependent on the presence or absence of S at the absorber surface. This approach is expected to be very useful in determining the electronic structure of real-world thin film surfaces from a variety of materials systems for energy conversion devices.

A4. Chemical structure of different interfaces in Cu(In,Ga)Se₂ thin film solar cell absorber structures

[Collaboration with K. Ramanathan, M. Contreras, and R. Noufi, National Renewable Energy Laboratory, NREL]

These investigations were based on two different samples, namely Cu(In,Ga)Se$_2$ "CIGSe"/Mo/glass and CdS/CIGSe/Mo/glass. To investigate also the interfaces buried beneath the absorber, namely the CIGSe/Mo interface and the Mo/glass interface, we prepared additional samples by cleaving the samples at those interfaces. For doing so, we have glued the front side of both samples to stainless steel plates and divided the stack into two parts. For the CIGSe/Mo/glass sample this cleavage takes place at the CIGSe/Mo-interface, as our measurements show. In contrast, the adhesion between Mo back contact and glass substrate was very weak for the investigated CdS/CIGSe/Mo/glass sample, such that this sample was cleaved at the Mo/glass interface. In total we thus had six different samples, which are schematically shown in Table III (the arrows show the direction of measurement):

Table III

Schematic presentation of the investigated sample surfaces/interfaces. Note that the arrows indicate the direction of measurement.

Sample	Name in the text	sketch
CIGSe/Mo/glass	CIGSe front	→ | CIGSe | Mo | glass
CIGSe/Mo/glass cleaved, top part	CIGSe back	CIGSe ← | Mo | glass
CIGSe/Mo/glass cleaved, bottom part	Mo front	CIGSe | → Mo | glass
CdS/CIGSe/Mo/glass	CdS	→ | CdS | CIGSe | Mo | glass
CdS/CIGSe/Mo/glass cleaved, top part	Mo back	CdS | CIGSe | Mo ← | glass
CdS/CIGSe/Mo/glass cleaved, bottom part	Glass front	CdS | CIGSe | Mo → | glass
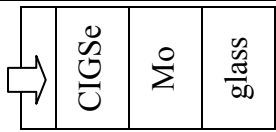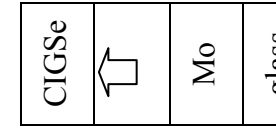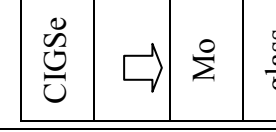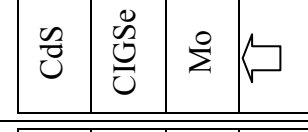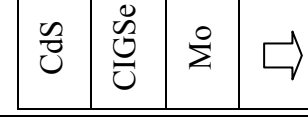
All samples were investigated by XES and the first three in the list also by XPS. Both techniques provide detailed information about the chemical properties of the investigated samples and complement each other with respect to their information depth (XES: bulk sensitive with an information depth of a
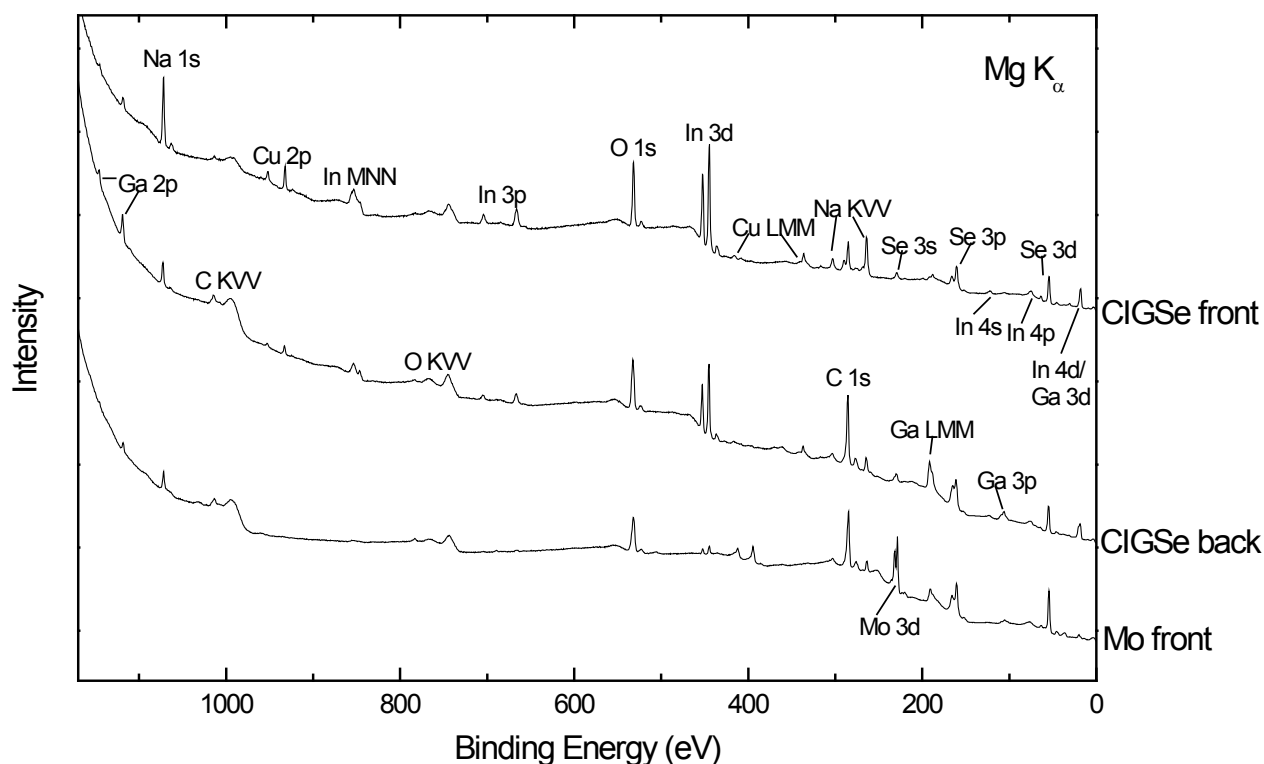
Fig. 20 *XPS survey spectra of the CIGSe front, the CIGSe back, and the Mo front of a Cu(In,Ga)Se$_2$ NREL absorber.*

few 100 nm, depending on the investigated line; XPS: surface sensitive with an information depth of a few nm).

Fig. 20 shows the XPS survey spectra of the CIGSe front, the CIGSe back and the Mo front. The names chosen for those samples are confirmed by those very surface sensitive spectra, since Mo is only found on the "Mo front" sample and not on the "CIGSe back" sample.

Since the samples were inevitably exposed to air prior to the measurements, a contamination layer consisting of C and O compounds is formed on their surface, complicating an exact quantitative analysis of the peak intensities. However, quite some qualitative information can be gathered from the XPS survey spectra shown in Fig. 20.

We find that the In 3d signal is stronger on the CIGSe front than on the CIGSe back side. This is because a higher amount of In is replaced by Ga at the absorber back side, which can be seen from the stronger Ga 2p signal at the absorber back side.

The Na amounts on the three samples differ strongly. The highest Na content is found on the absorber front side, whereas much less Na is located around the CIGSe/Mo interface represented by the two other samples.

27
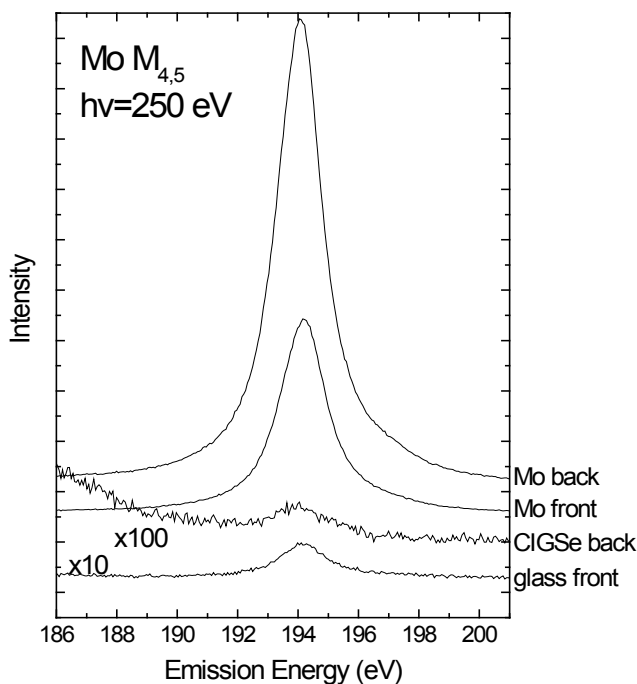
Fig. 21 *Mo M$_{4,5}$ XES spectra of Mo back, Mo front, CIGSe back, and glass front.*
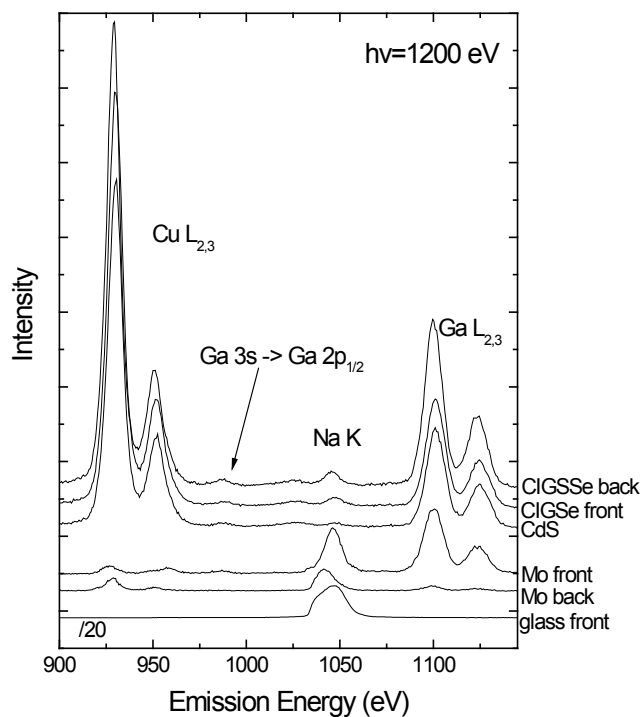
Fig. 22 *Cu L$_{2,3}$, Na K, and Ga L$_{2,3}$ spectra of all investigated samples.*

We find strong indications for different intermixing processes at the CIGSe/Mo interface, as will be discussed in the following. While only trace amounts of In and (within the detection limit of the experiment) no Cu is found, the Se signal increases at the Mo front side, pointing towards the formation of a MoSe$_2$ compound, as was found before for Cu(In,Ga)(S,Se)$_2$ absorbers [18]. This finding is corroborated by the Mo M$_{4,5}$ XES spectra shown in Fig. 21. Here the M$_{4,5}$ emission of the Mo front side is compared with that of the Mo back side (note that the spectra of the CIGSe back and the glass front only show some small Mo remainders). In accordance with the assignment to MoSe$_2$ (with a smaller Mo density than in metal Mo) the Mo signal is much weaker at the Mo front side.

Besides the Se diffusion, also a Ga diffusion into the back contact can be observed, which is manifested in the Ga 2p signal seen in the XPS survey spectrum of the Mo front side in Fig. 20. The more bulk sensitive XES measurements (mean free path of around 200 nm for energies around 1000 eV) in Fig. 22, where the Cu L$_{2,3}$, Na K, and Ga L$_{2,3}$ emission was recorded in one energy window, show that this Ga diffusion is very strong. While only small amounts of Cu can be found on the Mo front, the Ga L$_{2,3}$ intensity is more than half of that on the CIGSe back. The high Ga L$_{2,3}$ intensity found in the spectrum of the CIGSe back reveals that the Ga content at the CIGSe back compared to the CIGSe front is not only higher at those surfaces but in the whole surface near region.

From the Na K emission lines in Fig. 22, additional information about the Na distribution can be derived. The strongest Na signal is found on the soda lime glass substrate, as expected. In contrast to the surface sensitive measurements above, the Na signal at the CIGSe back is stronger than that at the CIGSe front, which can be explained as follows. It is known that Na at the CIGSe front is mainly localized at its

surface and only small amounts are found in the bulk or at grain boundaries near the front surface [19]. This localized Na gives a strong signal in the surface sensitive XPS measurements, whereas the Na content in the bulk and at grain boundaries next to the surface plays a more important role for the XES spectra. Therefore, the higher Na signal in the Na K XES spectra can be attributed to a higher Na content in the bulk region next to the back contact and/or at grain boundaries next to the CIGSe back.

In summary, we have investigated the CIGSe/Mo and Mo/glass interfaces by cleaving suitable samples. We suggest the formation of a $MoSe_2$ layer at the surface of the Mo back contact film. Furthermore, a strong Ga diffusion into the back contact can be observed. The actual compound formed during this diffusion and its role for the electronic structure and performance of the solar cell remains to be investigated in future experiments. Finally, we were able to draw a detailed picture of the Na distribution throughout the entire cell structure, showing Na mainly at the back side of the Mo back contact, at grain boundaries near the back contact, and, in particular, at the CIGSe front surface.

A5. The chemical and electronic structure of the deeply buried chalcopyrite/Mo interface

[Collaboration with S. Nishiwaki and W. Shafarman, Institute of Energy Conversion, IEC, U Delaware]

This work focuses on the deeply buried interface between absorber and Mo back contact in chalcopyrite thin film solar cells. These investigations were based on two different types of samples, namely CIGSe/Mo/glass and CIGSSe/Mo/glass. In order to make the interface between absorber and Mo accessible for characterization by photoelectron spectroscopy, we developed a suitable lift-off (cleavage) technique, which allowed us to cleave the absorber/Mo/glass samples at the desired interface. It was found that gluing the front side of the absorber/Mo/glass thin film stack to a stainless steel plate using a conductive (Ag-containing) UHV compatible epoxy allows a subsequent division of the stack in two parts and provides the necessary conductivity for the XPS, UPS, and IPES measurements. Note that the "lift-off" process itself took place in a N_2-filled glovebox or glovebag, which was directly connected to the load lock chamber of the UHV surface analysis system in order to minimize contamination of the freshly prepared cleavage planes. The scheme in Fig. 23 visualizes the different investigated surfaces for each lift-off process:

(a) Surface
(b) Back Surface
(c) Mo-Side
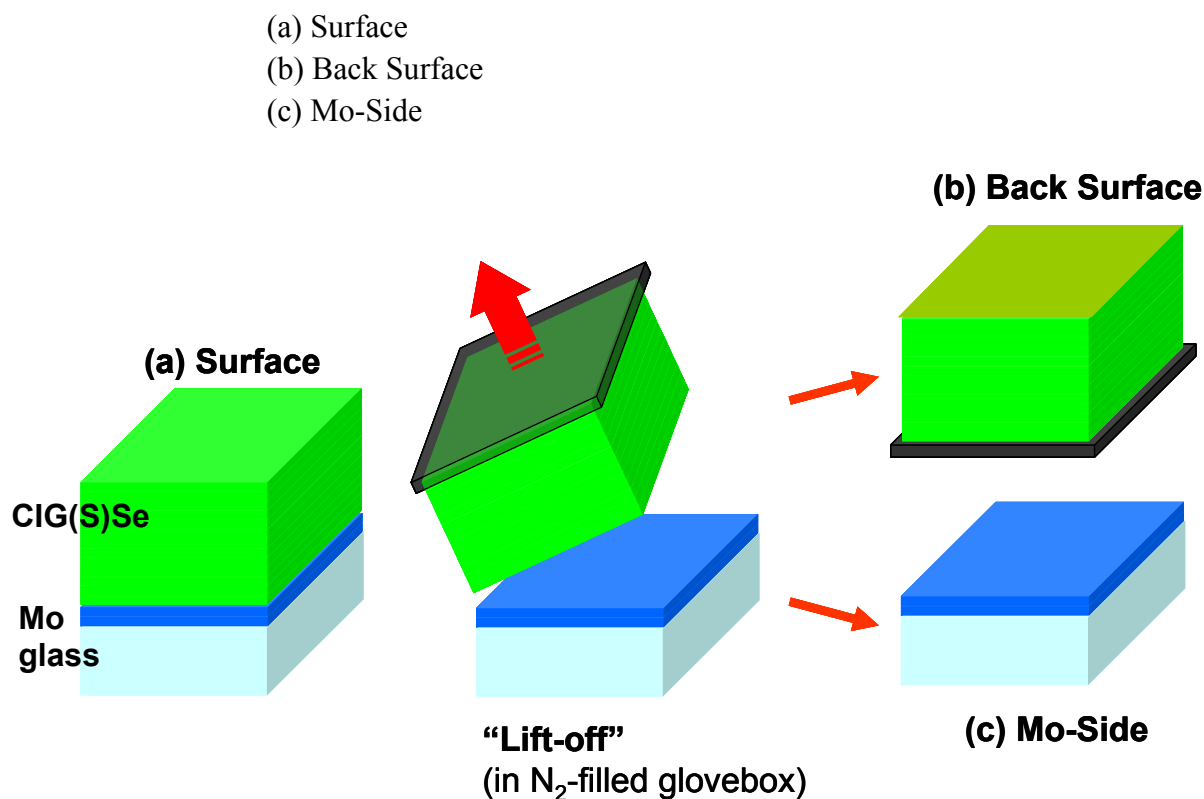
Fig. 23 *Scheme of the lift-off process and visualization of the different prepared and investigated surfaces.*

First, we will focus on the results gained from the investigation of the samples by XPS. Fig. 24 shows the XPS survey spectra of the Surface, Back Surface, and Mo-Side of the CIGSSe (top panel) and CIGSe (bottom panel) samples. Although the samples were handled and shipped under inert gas atmosphere and stored in UHV, one can observe distinct peaks which can be ascribed to C and O on the Surface (a), stemming from a contamination layer formed on the absorber surface. In contrast, we find only minor amounts of oxygen on the Back Surface (b). This shows that the applied cleavage process in an N_2 filled glovebag/glovebox and the immediate transfer of the cleaved samples into the attached UHV characterization system provides surfaces with minimized contamination (oxidation), which is of
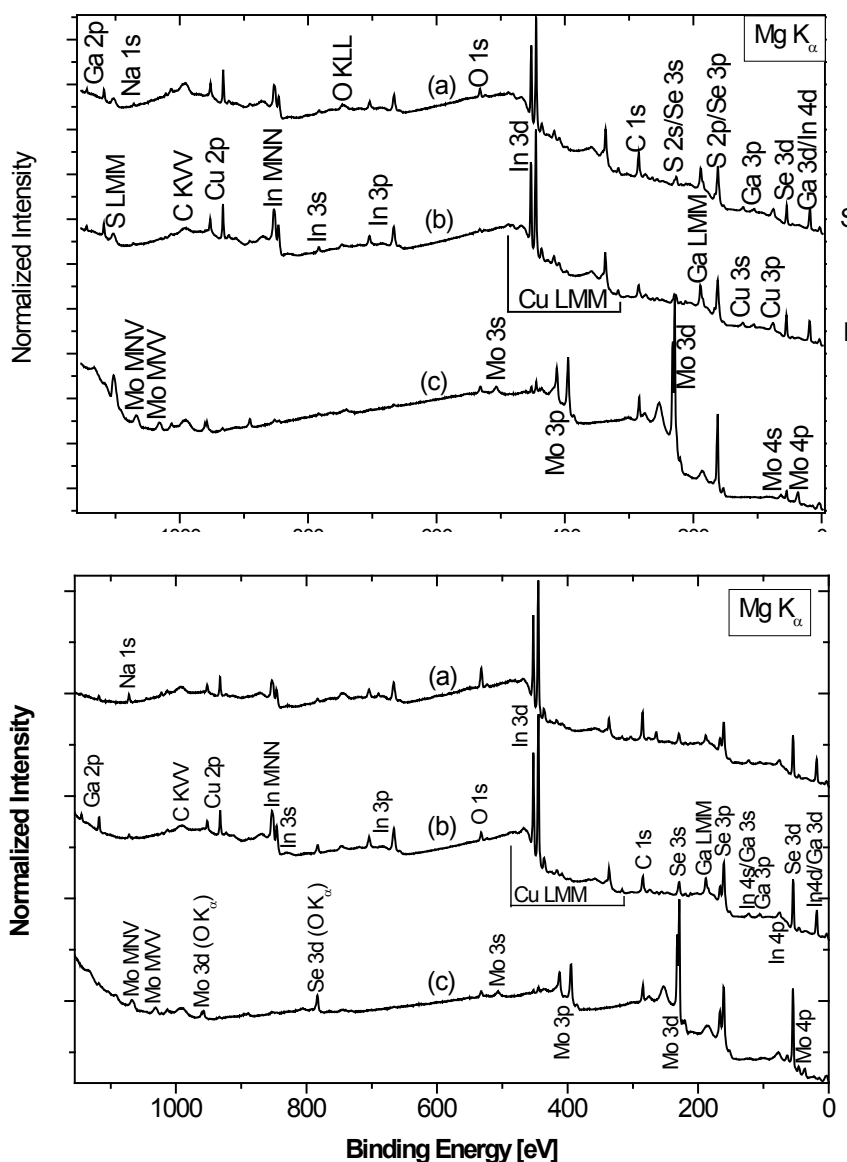
Fig. 24 *XPS survey spectra of the different accessible "surfaces" before and after lifting-off the chalcopyrite absorber from the Mo/glass substrate (top: CIGSSe, bottom: CIGSe): (a) Surface, (b) Back Surface, and (c)Mo-side.*

large importance for a subsequent determination of the electronic surface (and interface) structure. Note that the residual C 1s signal observed on the Back Surface points to a carbon incorporation into the absorber layer.

The intensity difference of all absorber features (e.g., Ga 2p, Cu 2p, and In 3d) between Surface and Back Surface can be explained by the different attenuation of the differently thick contamination layers. At first sight (see also discussion below) no Mo emission can be found on the Back Surface and only minor amounts of the absorber components (as indicated by the small In 3d peak - the most prominent absorber feature) can be observed on the Mo-Side. This confirms that the cleavage occurs at the absorber/Mo interface with only some chalcopyrite grains remaining on the back contact (this characteristic of the lift-off mechanism was already described in A4). In consequence, the comparatively large intensities of the photoemission and Auger lines of S and Se observed on the Mo Front point to the formation of a $Mo(S,Se)_2$ and $MoSe_2$ layer at the back contact for the CIGSSe and CIGSe sample, respectively. This was similarly reported/suggested in the past [20-25]. However, as shown in Fig. 25 (which shows the S 2p/Se 3p lines of the different CIGSSe-based samples), the S/Se ratio in the $Mo(S,Se)_2$ film does not mirror the S/Se ratio of the absorber. In this case, the formation of MoS_2 is clearly preferred over the formation of $MoSe_2$.
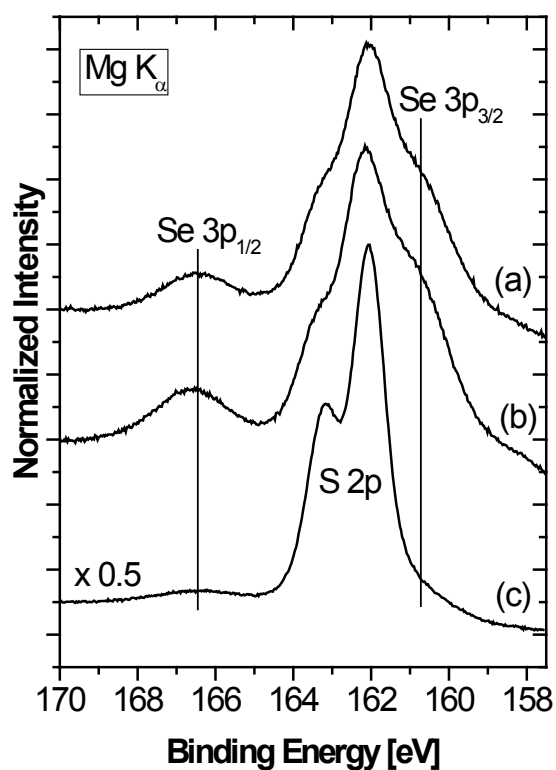
Fig. 25 *S 2p/ Se 3p photoemission of the different "surfaces" before and after lifting-off the CIGSSe absorber from the Mo/glass substrate: (a) Surface, (b) Back Surface, and (c)Mo-side.*
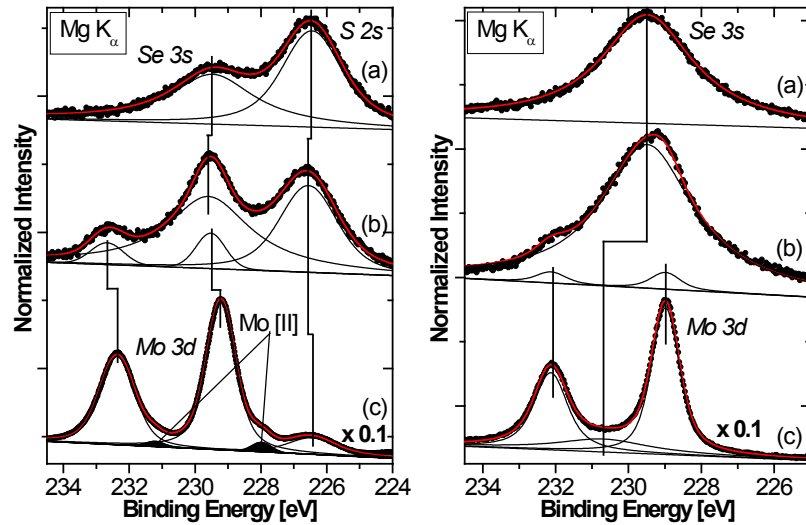
Fig. 26 *(Overlapping) S 2s/Se 3s and Mo 3d photoemission lines of the different "surfaces" before and after removing the chalcopyrite absorbers from the Mo/glass substrate (left: CIGSSe, right: CIGSe): (a) Surface, (b) Back Surface, and (c)Mo-side.*

A more detailed analysis of our data indicates that (besides the formation of the $Mo(S,Se)_2$) additional chemical interactions at the absorber/back contact interface take place. A detailed comparison of the S 2s/Se 3s and Mo 3d energy range for the different samples (Surface, Back Surface, Mo-Side, Fig. 26) reveals that a (minor) Mo signal at the Back Surface can be identified at both absorber/back contact structures. This agrees with our earlier X-ray emission (XES) measurements of different chalcopyrite/back contact structures (see A4), which also showed Mo at the absorber back side. It is at present unknown whether this is due to Mo diffusion into the Back Surface or the presence of some residual $Mo(S,Se)_2$ from the cleavage process.

A further important result from the spectra in Fig. 26 is the finding that the $Mo(S,Se)_2$ layer (in the CIGSSe case) is apparently thinner than the $MoSe_2$ layer (in the CIGSe case), as evidenced by the residual metallic Mo 3d doublet (filled black peaks in Fig. 26, bottom left) in the CIGSSe case.

Our previous XES data also showed an accumulation/diffusion of Ga at/into the back contact (see A4). Comparing the intensity of the most prominent photoemission lines of the absorber constituents (Ga $2p_{3/2}$, Cu $2p_{3/2}$, and In $3d_{3/2}$) of the Back Surface and the absorber remainders at the Mo-Side, our present XPS data confirms the accumulation of Ga. As shown in Fig. 27, we find that the Ga 2p intensity from the Mo-side is significantly larger than the intensity of the other absorber elements; note that the peaks in Fig. 27 were normalized to the absolute intensity of the respective peaks observed for the Back Surface, and hence a larger Ga peak directly indicates the presence of additional Ga on/in the Mo-side surface.
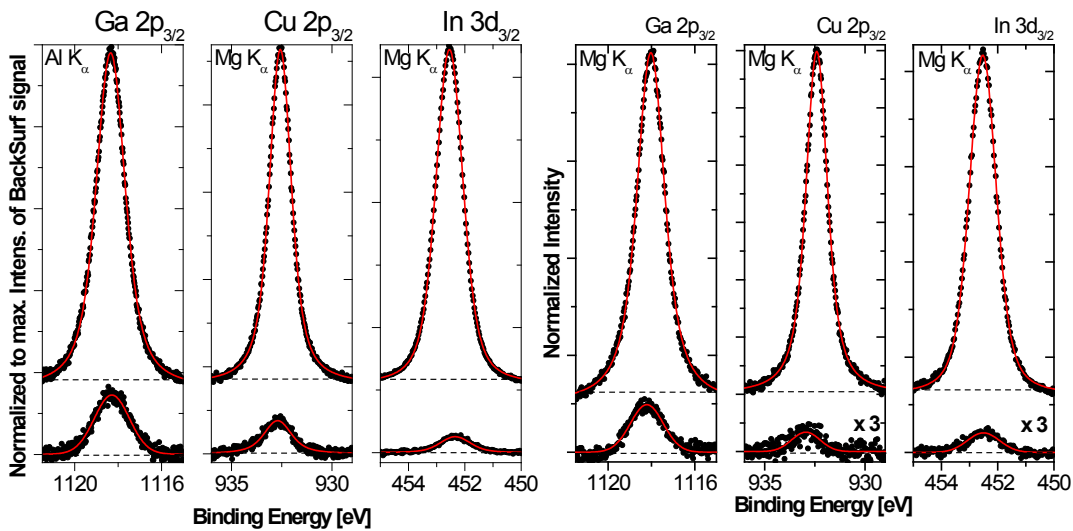
Fig. 27 *Comparison of the Ga 2p$_{3/2}$, Cu 2p$_{3/2}$, and In 3d$_{3/2}$ photoemission lines of the Back Surface (top) and absorber remainders at the Mo-Side (bottom). The intensities are normalized to the respective maximum of the Back Surface. The corresponding spectra of the CIGSSe/CIGSe samples are shown in the left and right three panels, respectively.*

In the following we will focus on the comparison of the CIGSSe Surface and CIGSSe Back Surface in terms of their composition. In order to determine the Ga/(Ga+In) = X and the S/(S=Se) = Y composition of the front and back side of the Cu(In$_{1-X}$Ga$_X$)(S$_Y$Se$_{1-Y}$)$_2$ absorber, the S 2p/Se 3p (Fig. 28) and the Ga 3d/In 4d detail spectra (Fig. 29) are evaluated. For direct comparison of CIGSSe Surface and CIGSSe Back Surface, the spectra are normalized to their maximum. In addition, the spectra of the latter have been shifted to lower binding energies by 0.1 eV for maximal overlap. The observed higher binding
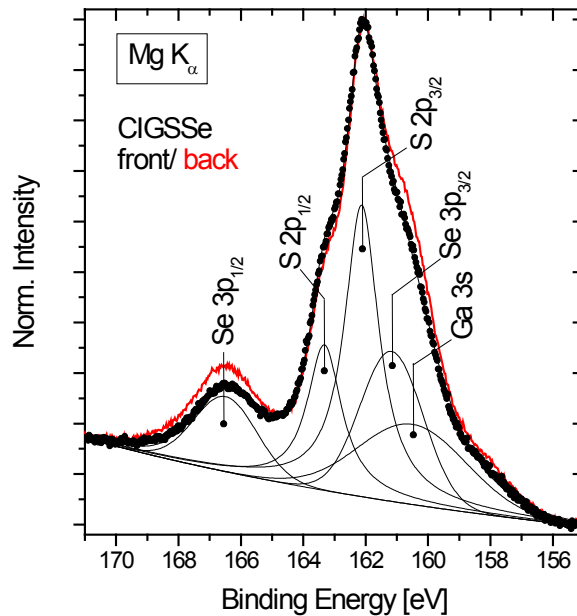
Fig. 28 *Region of the S 2p, Se3p, and Ga 3s photoemission lines of the CIGSSe Surface (black dots) and CIGSSe Back Surface (red line). For the CIGSSe Surface spectrum also the corresponding fits (black lines) are shown.*

energies for both, the S 2p/Se 3p and the Ga 3d/In4d spectra for the CIGSSe Back Surface point to an increased surface band bending compared to the CIGSSe Surface. Fig. 28 shows the region of the S 2p, Se 3p, and Ga 3s photoemission lines of the cleaved samples CIGSSe Surface (black dots) and CIGSSe Back Surface (red line). For the CIGSSe Surface spectrum also the corresponding fits (black lines) are shown. The comparison of the spectra clearly shows that the S/(S+Se) ratio at the CIGSSe Surface is higher than that of the CIGSSe Back Surface. For quantification of the S/(S+Se) ratio we have used the intensity of the S $2p_{3/2}$ and the Se $3p_{3/2}$ photoemission lines, which were determined by fitting the corresponding contributions of the spectra with Voigt area functions (exemplarily shown in Fig. 28). Due to the similar binding energies for the S 2p and the Se 3p peaks, it was legitimately assumed that the inelastic mean free paths and the analyzer characteristics are the same for the corresponding photoelectrons. Thus, for the calculation of the S/(S+Se) ratio the corresponding peak intensities were only corrected by the respective cross-sections (from Ref. [4]). In consequence, Y (the S/(S+Se) ratio) of the CIGSSe Surface and CIGSSe Back Surface was determined as 0.79 and 0.65, respectively, as shown in Table II. For the determination of X (the Ga/(Ga+In) ratio) of the CIGSSe Surface and CIGSSe Back Surface, we again have used adjacent photoemission lines (as shown in Fig. 29). The direct comparison of the Ga 3d/In 4d spectra of the cleaved samples CIGSSe Surface (black line) and CIGSSe Back Surface (red dots) reveals that X of both sample surfaces is quite similar. Indeed, the quantification of the Ga $3d_{5/2}$ and the In $4d_{5/2}$ photoemission lines determines X values (0.36 and 0.33, see Table IV) which are, within the error margins, identical for the CIGSSe Surface and CIGSSe Back Surface.

Table IV

Surface composition as determined by our XPS analysis.

sample	X Ga/(Ga+In)	Y S/(S+Se)	E_g [eV]
CIGSSe Surface	0.36	0.79	1.68
CIGSSe Back Surface	0.33	0.65	1.58

Assuming a stoichiometric absorber composition (in particular no Cu deficiency towards the absorber surface) the X and Y compositions should allow a direct ("theoretical") estimate of the absorber band gap (E_g). Using equation (6) (Ref. [8]) we have determined E_g for the CIGSSe Surface to 1.68 eV and for the CIGSSe Back Surface to 1.58 eV (see Table IV).

$$E_g = 1 + 0.13X^2 + 0.08X^2Y + 0.13XY + 0.55X + 0.54Y \qquad (6)$$
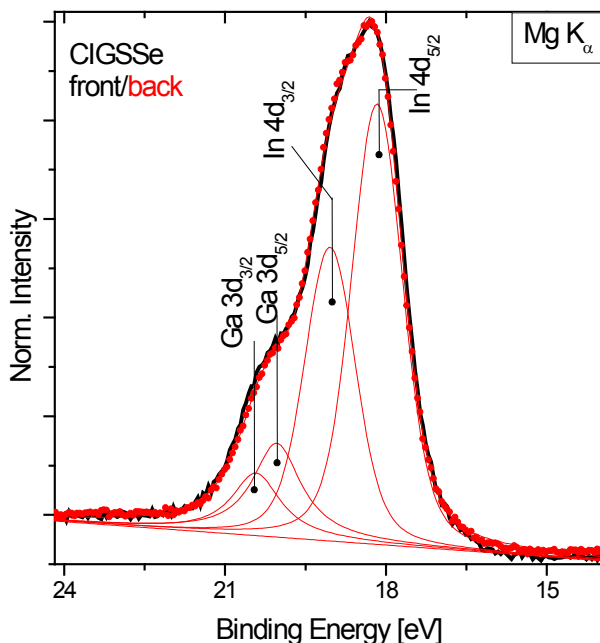
Fig. 29 *Ga 3d and In 4d spectra of the cleaved samples CIGSSe Surface (black line) and CIGSSe Back Surface (red dots). For the CIGSSe Back Surface spectrum also the corresponding fits (red lines) are shown.*

In order to directly *measure* the band gap at the CIGSSe Surface and CIGSSe Back Surface, we additionally characterized a set of cleaved samples with UV photoelectron spectroscopy (UPS) and inverse photoemission (IPES). The corresponding UPS and IPES spectra for the CIGSSe Surface and Back Surface are shown in Fig. 30 left and right, respectively. The linear extrapolation of the leading edge of the UPS and IPES spectra results in the position of the valence band maximum (VBM) and conduction band minimum (CBM), respectively. Thus, the sum of the absolute values of VBM and CBM reveals the electronic surface band gap E_g^{Surf}. In addition to the UPS/IPES spectra and the respective VBM, CBM, and E_g^{Surf} values of the as-prepared CIGSSe Surface (left) and CIGSSe Back Surface (right) samples, Fig. 30 also shows the electronic properties after several cleaning cycles with a mild Ar^+ beam (E_{ion} = 50 eV, I_{sample} < 1μA). As can be observed in Fig. 30, the VBM, CBM, and E_g^{Surf} values remain constant after 30 min (CIGSSe Back Surface) and 60 min (CIGSSe Surface) of Ar^+ treatment. The difference in required treatment time is most likely due to the more pronounced contamination layer on the CIGSSe Surface, as discussed above. The respective XPS survey spectra after Ar^+ treatment (not shown) also indicate clean sample surfaces without C- or O-containing contaminants. The experimentally determined electronic surface band gaps of (1.94 ± 0.15) eV for the CIGSSe Surface and (2.09 ± 0.15) eV for the CIGSSe Back Surface are larger than the band gaps calculated from the surface stoichiometry determined by XPS (see Table IV). Enlarged electronic surface band gaps have in the past [6,12,13] been explained by the formation of a Cu-poor "Ordered Vacancy Compound" [26] or "Ordered Defect Compound" [27] surface phase, which deviates from the Cu : In+Ga : S+Se ratio of 1 : 1 : 2 forming on top of the chalcopyrite absorber. Our XPS results indeed show a Cu-poor surface stoichiometry for both, the CIGSSe Surface as well as the CIGSSe Back Surface. However, it is not clear whether the Cu-poor surface phase at the CIGSSe Back Surface is present from the beginning or whether its formation is induced by the lift-off process and subsequent exposure to N_2 atmosphere in the glovebox/glovebag or UHV, respetively.
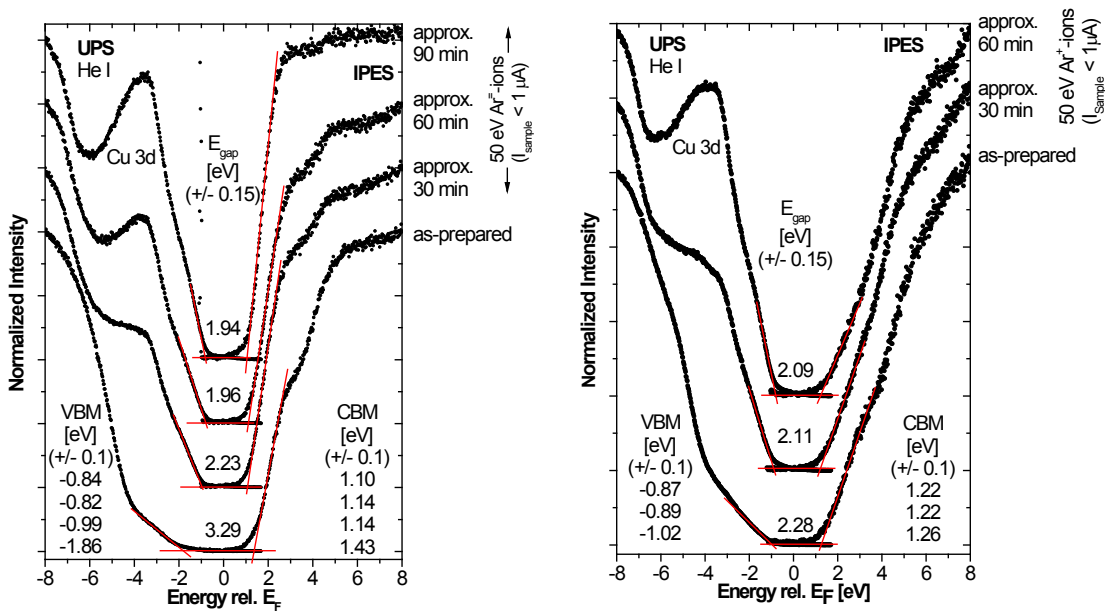
Fig. 30 *UPS and IPES spectra (black dots) and derived VBM, CBM, and surface band gap values of as-prepared CIGSSe Surface (left) and CIGSSe Back Surface (right) samples. In addition, the corresponding spectra are also shown after different cleaning steps by a mild (50 eV Ar$^+$) sputter cleaning. The solid red lines represent the linear extrapolation of the leading edge of the respective spectra. Note that "0" on the energy scale indicates the position of the Fermi edge E_F.*

In the past it was discussed whether the chalcopyrite/Mo interface results in an Ohmic contact [23,28,29] or whether a Schottky contact [30,31] is formed. Kohara *et al.* even suspected the observed MoSe$_2$ layer to be responsible for an Ohmic contact at the chalcopyrite/Mo interface [23]. In a conventional CIGSSe-based solar cell device the charge carriers are generated in the low-gap, p-type chalcopyrite absorber and are separated in the electric field caused by the pn-junction formed by depositing the wide-gap, n-type window material onto the absorber. Thus, the photogenerated electrons (holes) have to travel to the front (back) contact to be able to contribute to the photocurrent. In consequence, the bandoffset of the valence band at the CIGSSe/Mo interface has to be known in order to judge the quality of the interface in terms of unhindered current transport. Hence, in order to shed more light on the electronic properties of the chalcopyrite/Mo interface, also the CIGSSe Mo-side was additionally characterized by UPS and IPES. The corresponding spectra of a freshly cleaved sample are shown in Fig. 31. Again the VBM and CBM are determined by linear extrapolation of the leading edges of the UPS and IPES spectrum, respectively. The resulting surface band gap of (1.30 ± 0.15) eV agrees surprisingly well with that of MoS$_2$ (1.20 – 1.35 eV [32]), which confirms the preferred formation of MoS$_2$ over that of MoSe$_2$ at the CIGSSe/Mo interface as discussed above.
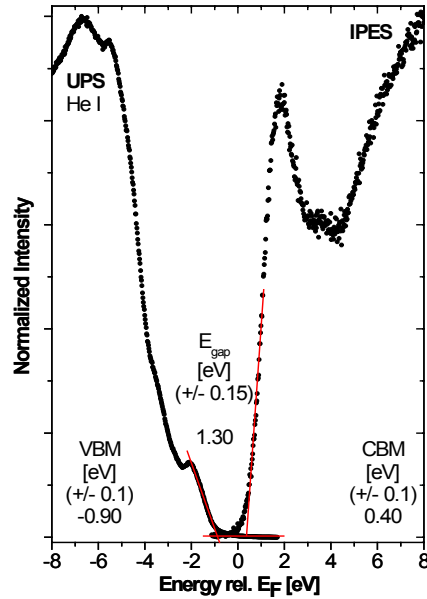
Fig. 31 *UPS and IPES spectra (black dots) and VBM, CBM, and surface band gap values of a freshly cleaved CIGSSe Mo-Side sample. The solid red lines represent the linear approximation of the leading edge of the respective spectra. Note that "0" on the energy scale indicates the position of the Fermi edge E_F.*
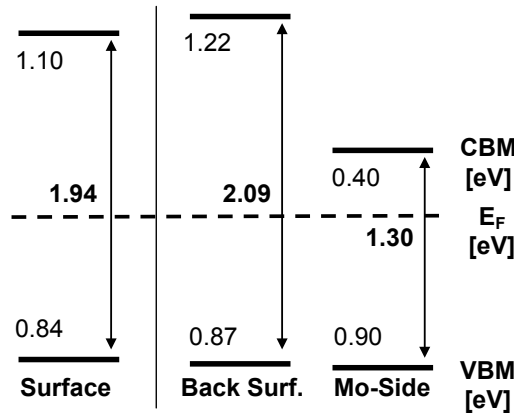
Fig. 32 *Schematic summary of the valence band maxima (VBM), conduction band minima (CBM), electronic surface band gaps, and Fermi energy position. All numbers are given in eV and have an error of 0.10 eV (VBM and CBM) and 0.15 eV (band gaps).*

The scheme in Fig. 32 shows a summary of the positions of the valence band maxima, the conduction band minima and the surface band gaps for all investigated samples. Neglecting any potential interface-induced band bending, Fig. 34 shows that the valence band at the CIGSSe/Mo(S$_2$) interface is (within the error bars) aligned and thus no barrier for hole transport across that interface is present. Furthermore, the conduction band at the CIGSSe Back is slightly higher than at the CIGSSe Surface, possibly suggesting the presence of a "back surface field" that repels minority charge carriers (electrons) from the CIGSSe/Mo interface.

Based on our investigations it is – for the first time – possible to draw a complete picture of the chemical and electronic properties of the deeply buried chalcopyrite/back contact interface. We have found a pronounced chemical interaction between absorber and back contact, namely the formation of $MoSe_2$ (and $Mo(S,Se)_2$) and a "diffusion" of Ga into the Mo layer. In addition, we could (tentatively) derive a flat valence band alignment at this interface.

B1. The chemical structure of the CdTe/CdS interface investigated by XES

[Collaboration with the group of A. Compaan, U Toledo]

These investigations were based on two sets of samples, namely differently treated CdS thin films and CdTe/CdS thin film stacks, respectively (see Table V for a complete list). For the latter set of samples, the impact of $CdCl_2$-treatment on the CdTe/CdS thin film stacks was investigated, while for the CdS thin films also the influence of Cu-diffusion was analyzed. In addition, some powder samples (CdS, $CdSO_4$, $CdCl_2$) were characterized for comparison.

Table V

In total, we thus investigated eight different samples.

Sample	Treatment	Name in the text
CdS (thin film on glass)	none	as-grown CdS
CdS (thin film on glass)	$CdCl_2$-treated	$CdCl_2$-treated CdS
CdS (thin film on glass)	Cu-diffused	Cu-diffused CdS
CdTe/CdS (thin film stack on glass)	none	as-grown CdTe/CdS
CdTe/CdS (thin film stack on glass)	$CdCl_2$-treated	$CdCl_2$-treated CdTe/CdS
$CdSO_4$, CdS, $CdCl_2$ (powders)	N/A	$CdSO_4$, CdS, $CdCl_2$ references

All samples were investigated by X-ray emission spectroscopy (XES). As mentioned above, this technique provides detailed information about the chemical properties of the investigated samples, and, as a photon-in photon-out technique, probes the "near-surface" bulk. In our case, where we have focused on the S $L_{2,3}$ and Cl $L_{2,3}$ emission, XES has an information depth of about 100 nm.

Fig. 33 shows the S $L_{2,3}$ XES spectra of the set of CdS samples. At first sight, all spectra look identical. The main feature (1) at 147.3 eV (which is actually a doublet indicated by the clearly visible shoulder at 149 eV) can be ascribed to S 3s electrons decaying into S $2p_{1/2}$ and S $2p_{3/2}$ core holes. In addition, the two peaks at 150.5 eV and 151.8 eV (2) correspond to Cd 4d electrons decaying into the S $2p_{1/2}$ and S $2p_{3/2}$ core holes, respectively, and thus indicate sulfur atoms bound to Cd. Furthermore, we observe the upper valence band of CdS at about 156 eV. Altogether, all spectra show the typical features of a S $L_{2,3}$ spectrum of CdS, which is also confirmed by the respective spectrum of the CdS reference. However, a close inspection of the data shows small but significant differences for, e.g., the S $L_{2,3}$ XES spectrum of
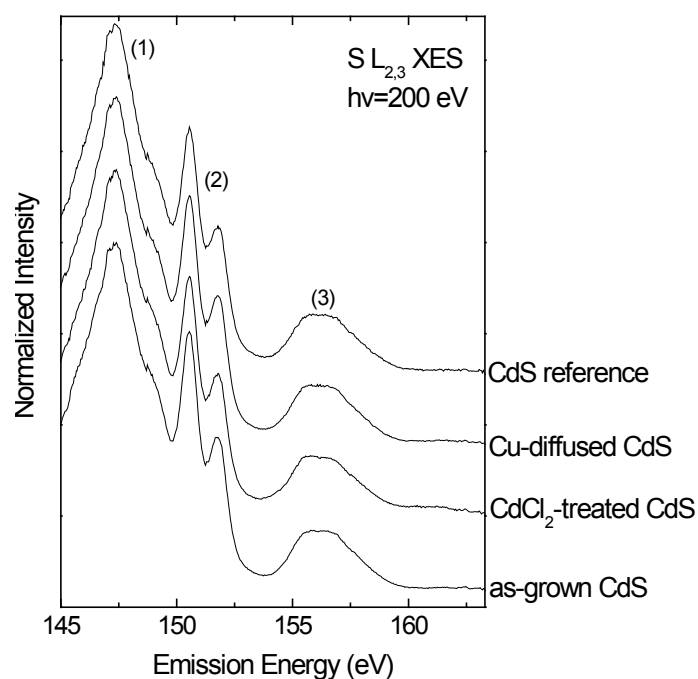
Fig. 33 *S $L_{2,3}$ XES spectra of a set of differently treated CdS thin films. In addition, a corresponding spectrum of a CdS reference is also shown (top spectrum). The main features are labeled (1) – (3).*

the as-grown CdS (a) compared to that of the Cu-diffused CdS sample (b), as shown in Fig. 34. In Fig. 34, the raw spectra and the corresponding difference spectrum are shown. The comparison of the (enlarged) difference (a)-(b) with a CdS and a $CdSO_4$ reference spectrum reveals that the features in the difference spectrum can be ascribed to the formation of S-O bonds and a localization of the Cd 4d-derived band.

The spectra of the differently treated CdTe/CdS thin film stacks are shown in Fig. 35. Since the thickness of the CdTe layer, which covers the CdS, is significantly beyond the information depth of XES, one would not expect to observe a S $L_{2,3}$ signal. This is indeed the case for the as-grown CdTe/CdS thin film stack. However, the S $L_{2,3}$ spectrum of the $CdCl_2$-treated CdTe/CdS sample clearly shows some small (note the magnification factor) spectral features, which are similar to the CdS spectra shown in Fig. 33. A comparison with the spectrum of the as-grown CdS thin film as well as with the $CdSO_4$ reference reveals that the S $L_{2,3}$ spectrum of the $CdCl_2$-treated CdTe/CdS thin film stack can be described as a superposition of spectral features of both reference samples. Most prominently, the two peaks at 150.5 eV and 151.8 eV directly indicate S-Cd bonds, and the peaks at 153.9 eV, 155.1 eV, and 161.0 eV can be directly ascribed to S-O bonds. In consequence, this points to a $CdCl_2$-treatment-induced crack or void formation of the CdTe layer or, more likely, to a strong intermixing (the latter is commonly accepted in the community). For the CdTe/CdS thin film stacks we also investigated the Cl $L_{2,3}$ XES spectra, as shown in Fig. 36 (multiplied by the given magnification factors). The two major features of the observed spectra at 182.3 eV and 183.8 eV can again be ascribed to 3s electrons decaying into the $2p_{1/2}$ and $2p_{3/2}$ core holes, this time for electrons in Cl. As expected, we find a Cl $L_{2,3}$ XES spectrum for the $CdCl_2$-treated CdTe/CdS sample (middle spectrum in Fig. 36), the main features of which are quite similar to those of the $CdCl_2$ reference. The fact that the structures between 185 and 190 eV and between
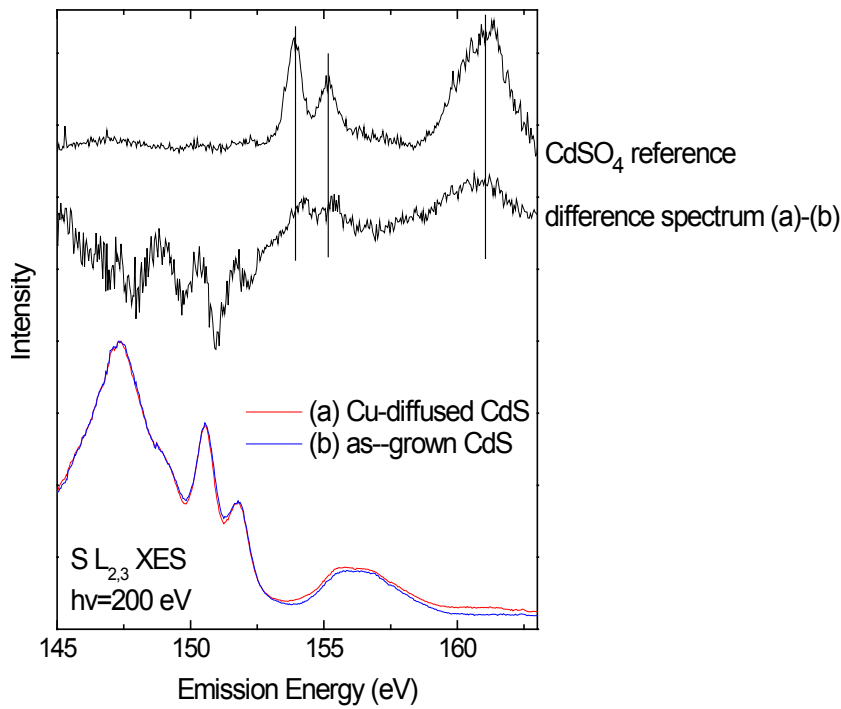
Fig. 34 *S L$_{2,3}$ XES spectra of a Cu-diffused CdS thin film (a) plotted upon that of an as-grown CdS sample (b). In addition, the corresponding (enlarged) difference spectrum (a-b) and a CdSO$_4$ reference spectrum is also shown.*
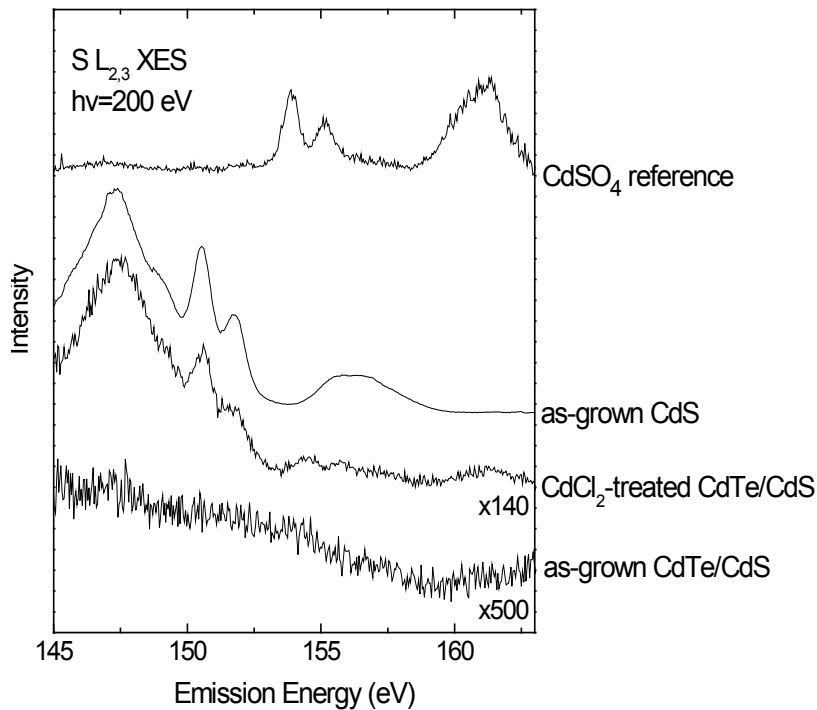
Fig. 35 *S L$_{2,3}$ XES spectra of a set of differently treated CdTe/CdS thin film stacks. In addition, the corresponding spectrum of an as-grown CdS thin film and a CdSO$_4$ reference spectrum are also shown. Note the different magnification factors.*
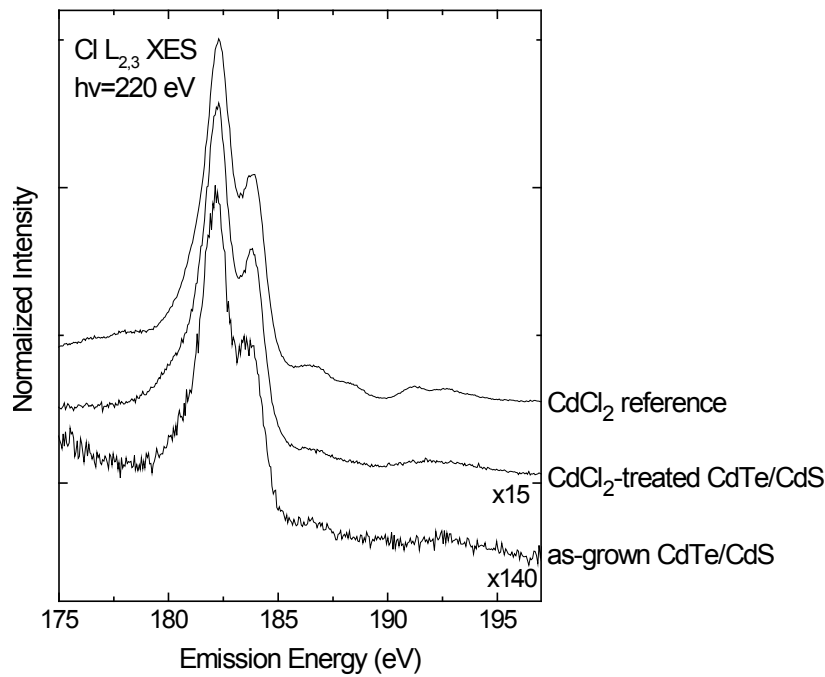
Fig. 36 *Cl L$_{2,3}$ XES spectra of a set of differently treated CdTe/CdS thin film stacks. In addition, the corresponding spectrum of CdCl$_2$ reference spectrum is also shown. Note the different magnification factors.*

190 eV and 194 eV are less pronounced than in the reference sample, indicates the presence of Cl atoms that are not directly bound to Cd. Surprisingly, one can also identify a weak (note the magnification factor) Cl L$_{2,3}$ XES spectrum for the as-grown CdTe/CdS thin film stack, which shows all the characteristics of CdCl$_2$. Whether this is due to extrinsic contamination or a result of the used sample preparation (and thus significant) is the topic of future experiments.

Based on these results, we will continue the investigation of these CdTe/CdS samples and extend them by investigating customized sample series with UPS and IPES to get insight into the band alignments at the various interfaces of the device structure of the CdTe-based solar cell.

B2. The chemical structure of the CdTe/CdS interface investigated by XPS

[Collaboration with the group of X. Wu, National Renewable Energy Laboratory, NREL]

In order to become familiar with the special characteristics of CdTe/CdS samples with respect to their investigation in photoemission measurements, we conducted first XPS measurements of CdTe/CdS samples prepared by the group of X. Wu (NREL). The first set of test structures consisted of the following samples:

Table VI

Complete list of investigated samples.

Sample	Treatment	Name in the text
CdTe/CdS (thin film stack on glass)	none	#1
CdTe/CdS (thin film stack on glass)	$CdCl_2$-treated and etched	#3
CdTe/CdS (thin film stack on glass)	$CdCl_2$-treated	#4
Cu (5nm)/CdTe/CdS (thin film stack on glass)	Before Cu deposition: $CdCl_2$-treated and etched After Cu deposition: None	#5
Cu (150nm)/CdTe/CdS (thin film stack on glass)	Before Cu deposition: $CdCl_2$-treated and etched After Cu deposition: None	#6
Cu (5nm)/CdTe/CdS (thin film stack on glass)	Before Cu deposition: $CdCl_2$-treated and etched After Cu deposition: Annealing for 30s @ 250ºC	#7
Cu (150nm)/CdTe/CdS (thin film stack on glass)	Before Cu deposition: $CdCl_2$-treated and etched After Cu deposition: Annealing for 30s @ 250ºC	#8

In view of the high surface sensitivity of XPS, all samples showed significant surface contamination (see discussion below), prohibiting a meaningful subsequent characterization by UPS or IPES. However, there is evidence that the contamination (oxidation) is concentrated at the surface, most likely caused by exposing the samples to ambient air. This indicates that with proper sample handling and, possibly, a low-energy (50 eV) ion desorption step, sufficiently clean surfaces can be obtained. The fact that Te is indeed only oxidized at the sample surface is confirmed by the Te $3d_{3/2}$ spectra shown in Fig. 37 (left). All spectra show a significant high binding energy feature at approx. 587 eV, indicative for oxidized tellurium, except the corresponding spectrum of sample #6. Here, the tellurium is covered by a thick
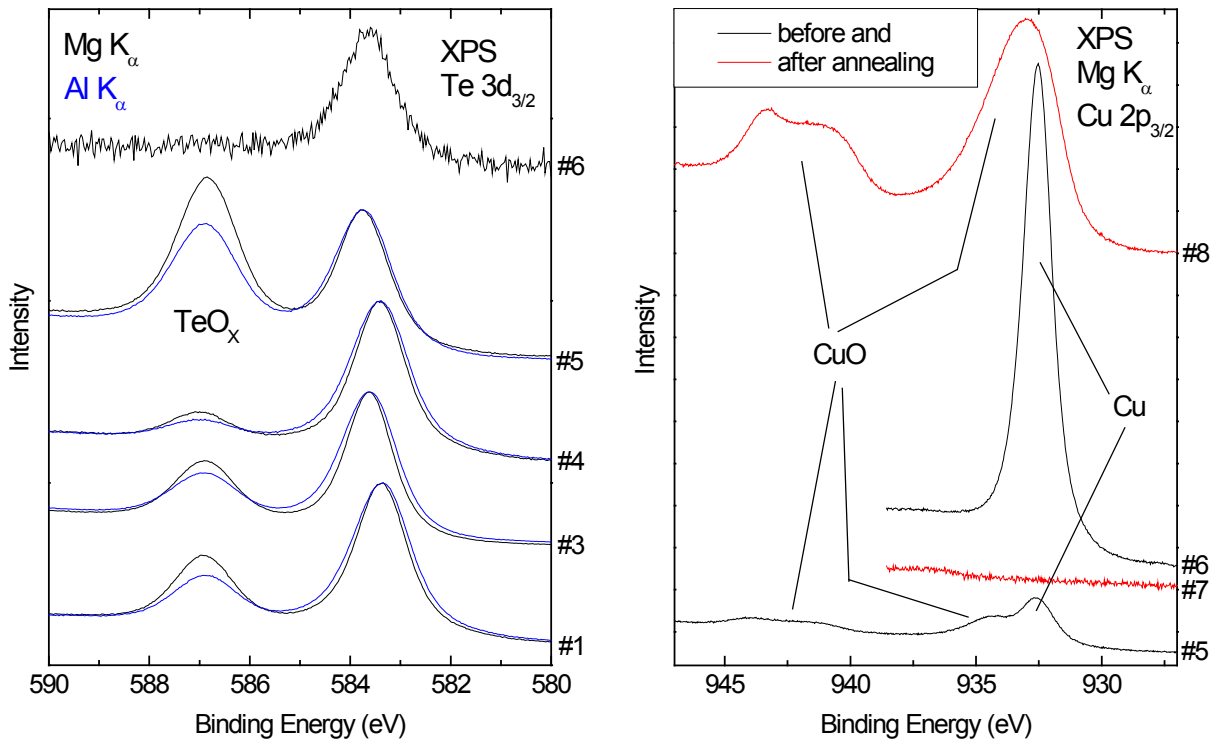
Fig. 37 *Detail spectra of the Te 3d$_{3/2}$ (left) and Cu 2p$_{3/2}$ (right) photoemission line of the different investigated CdTe/CdS thin film stacks.*

[nominal 150 nm] Cu layer preventing its oxidation. (Note that a tellurium XPS-signal is visible "through" the thick Cu layer, which is a strong indication that the Cu does not cover the underlying CdTe completely.) The "buried" non-oxidized tellurium indicates that the oxidation takes place after the actual production process. Furthermore, the graph shows the Te 3d$_{3/2}$ photoelectrons not only excited with Mg K$_\alpha$ (hν = 1253.6 eV) but also with Al K$_\alpha$ excitation (hν = 1486.6 eV). Using Al K$_\alpha$ excitation, the electrons have a higher kinetic energy and thus according to the "universal curve" of the inelastic mean free path (IMFP) [17] a larger IMFP. Therefore, the corresponding spectra (Fig. 39 (left), blue) are less surface sensitive. It can be observed that the intensity of the TeO$_x$ component (high binding energy feature) in those spectra is smaller as compared to that of the respective spectra conducted with Mg K$_\alpha$ excitation, also confirming that the tellurium is only oxidized at the sample surface.

An additional interesting result is shown in Fig. 37, right. While sample #6 (thick [nominal 150 nm] Cu layer on the CdTe/CdS stack) shows metallic Cu, the very thin [nominal 5nm] Cu film of sample #5 is partly oxidized, as indicated by a second peak at higher binding energies around 943 eV. The spectra clearly show the presence of CuO, since, for Cu$_2$O, the peak would only be shifted by ~1 eV to higher binding energies with respect to the Cu 2p$_{3/2}$ photoemission line of metallic Cu. Furthermore, for CuO two peaks as observable in the present case are typical. In addition, it can be observed that after annealing of the Cu/CdTe/CdS thin film stacks the thin Cu layer is vanished (compare spectra of samples #5 and #7 Fig. 37, right) and the thick Cu layer is also partly oxidized (compare spectra of samples #6 and #8 Fig. 37, right), respectively.

C1. Chemical surface structure of CIGSe absorbers on stainless steel
[Collaboration with Global Solar Energy Inc.]

Surprisingly, very little is known about the chemical and electronic structure in *real-world industrial-grade* samples, i.e., manufactured in large-scale, high-throughput equipment in an industrial environment. Global Solar Energy, Inc. ("GSE"), e.g., has pioneered a unique robust process to manufacture CIGSe solar cell devices which can hardly be simulated on laboratory scale. While other companies pursue the approach of in-line deposition on rigid glass substrates, GSE is the only company to date using a roll-to-roll coating of the complete solar cell thin film layer stack on flexible substrates. Central questions of the latter approach are how the chemical structure of the deposited materials differs from that of conventionally prepared materials and how the process-specific parameters influence the material properties. The roll-to-roll process itself presents a set of process-specific challenges as well, such as chemical interactions between the deposited material (front side) and the back side of the flexible substrate during roll-up after each preparation step.

In order to investigate the material properties in CIGSe-based thin film solar cells induced by roll-to-roll deposition on flexible substrates a set of samples directly taken out of the production process of Global Solar Energy, Inc. ("GSE") was investigated. For the different samples which represent the status after individual deposition steps in the manufacturing process, both, the front and back side was investigated by XPS.

Fig. 38 shows respective schemes of the investigated test structures. Shown is a typical structure used by GSE for their commercial PV process. Different materials are being utilized at GSE for the top electrode. In this specific case ZnO and ITO was used.
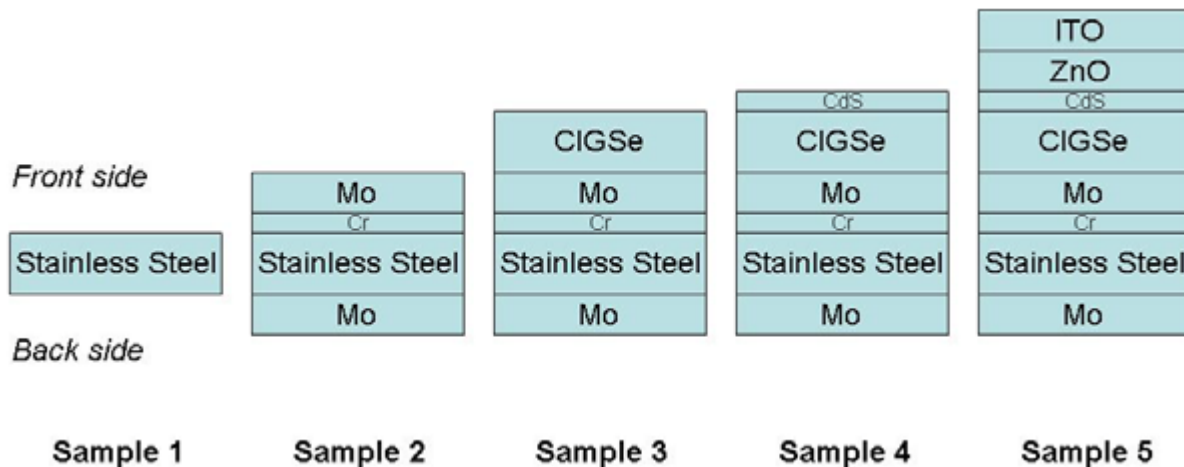
Fig. 38 *Schemes of the investigated samples.*
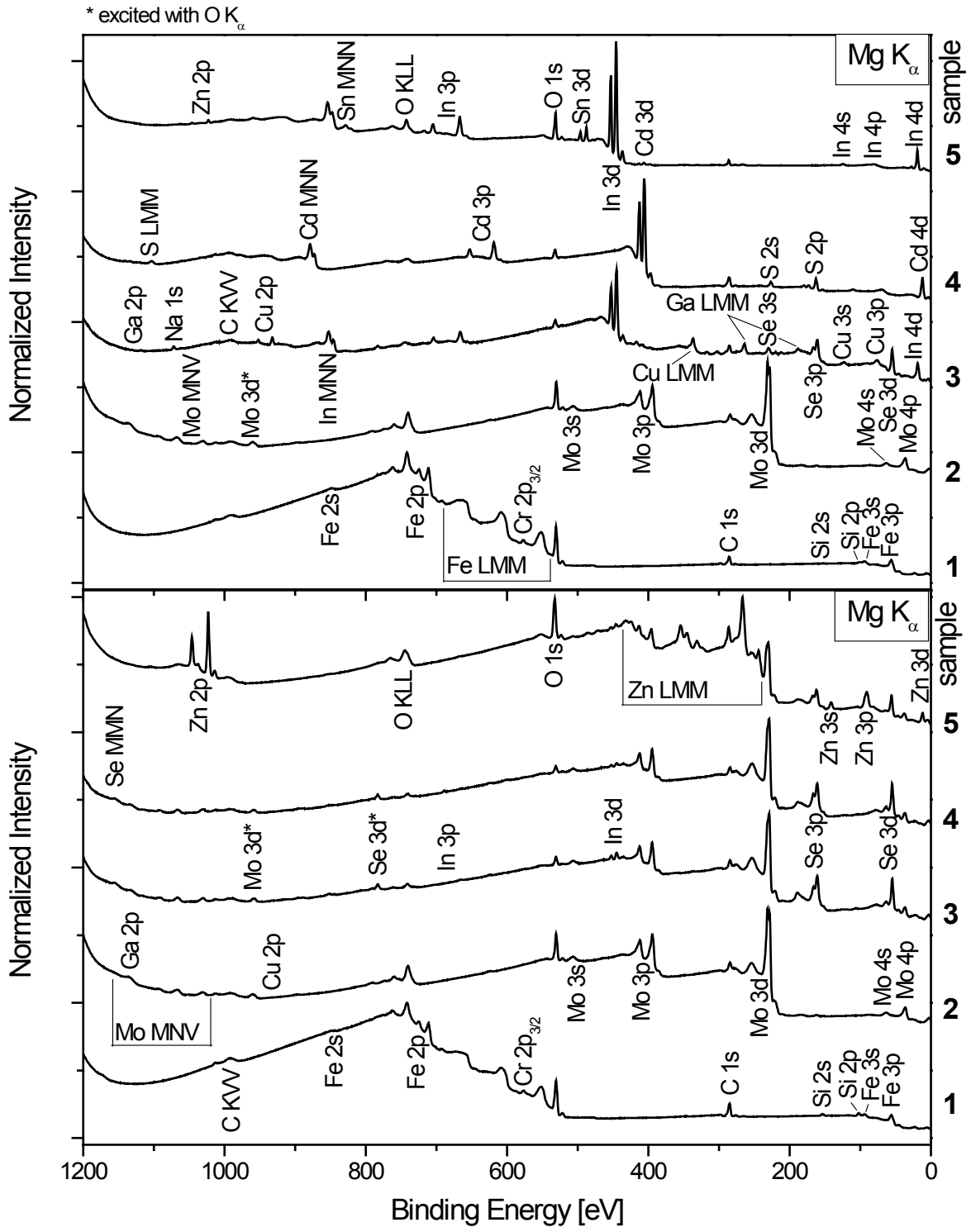
Fig. 39 *XPS survey spectra of the front (top panel) and back side (bottom panel) of the investigated test structures.*
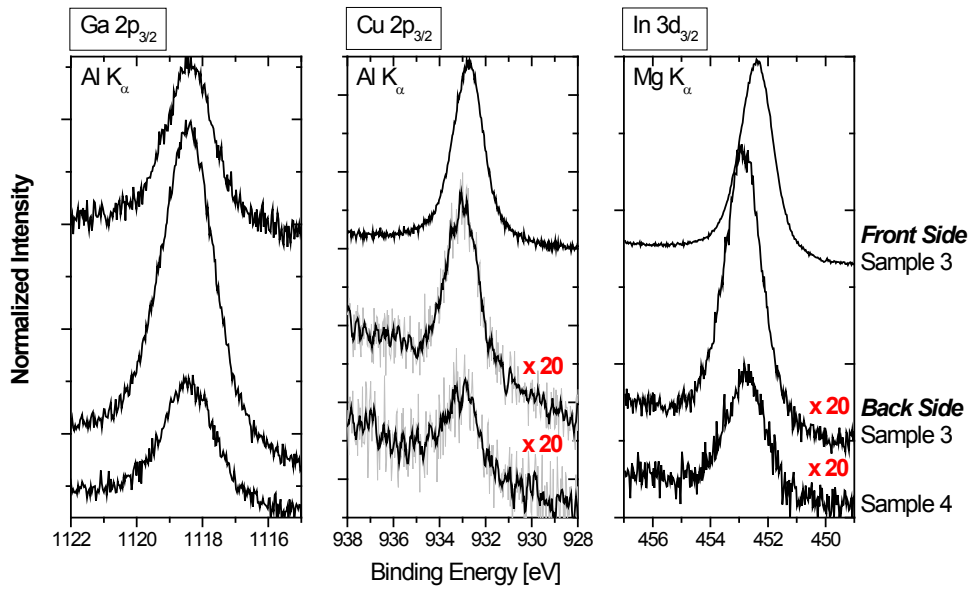
Fig. 40 *XPS Ga 2p₃/₂ (left), Cu 2p₃/₂ (center), and In 3d₃/₂ (right) detail spectra of the front side sample #3 (top spectra) and the back side samples #3 and #4 (bottom two spectra).*
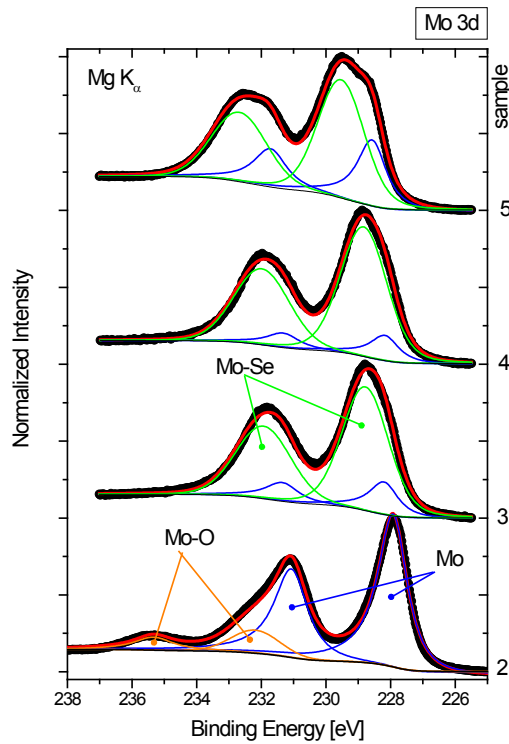
Fig. 41 *XPS Mo 3d detail spectra of the back side samples #2-5 (experimental data shown as dots, fits indicated by solid lines).*

Fig. 39 shows the survey spectra of the front (top panel) and back side (bottom panel) of the investigated test structures. For the front side samples we find the elements of the respective deposited material. As indicated by the small C 1s (and O 1s) XPS peak the surface contamination could successfully be

minimized due to a suitable packaging and shipping procedure. We find a relatively high amount of oxygen on sample #2, which points to the formation of MoO_x. The back side samples (except #1) are dominated by Mo-related XPS signals. Surprisingly, we find a relatively high amount of selenium for samples #3 - #5 which is indicative for the formation of $MoSe_2$ upon absorber formation (see also detail spectra in Fig. 41). Furthermore, we find CIGSe-related XPS peaks on back side sample #3 and #4 (see also the detail spectra in Fig. 40), which are explained by an interaction of front side absorber material with the back side during roll-up of the stainless steel tape after CIGSe deposition.

The comparison of the Ga $2p_{3/2}$, Cu $2p_{3/2}$, and In $3d_{3/2}$ detail spectra of the front side sample #3 and the back side samples #3 and #4 in Fig. 40 shows an abundance of Ga at the back side sample surfaces (note the magnification factors indicated for the Cu $2p_{3/2}$ and In $3d_{3/2}$ XPS peaks of the back side samples). This can be interpreted not only as a simple deposition of front side material on the back side, but indicates a significant chemical interaction leading to the observed Ga accumulation.

Fig. 41 shows the XPS Mo 3d detail spectra of the back side samples #2-5. For all spectra, we find pronounced spectral features which deviate from a Mo 3d spectrum of a single Mo species. By peak fitting the spectra of sample #1, we were able to identify two Mo 3d doublets which we ascribe to metallic Mo and Mo-O bonds, respectively. As indicated by the pronounced change in the spectral shape of the Mo 3d spectra after CIGSe deposition (sample #3) and confirmed by our peak fit analysis, the (oxidized) Mo is converted into $MoSe_2$ upon absorber formation. The fact that the metallic Mo 3d doublet is still visible indicates that the $MoSe_2$ layer might not be closed or too thin (i.e., thinner than the XPS information depth) to completely attenuate the Mo 3d photoelectrons stemming from the underlying metallic Mo.

References

[1]   I. Repins, M.A. Contreras, B. Egaas, C. DeHart, J. Scharf, C.L. Perkins, B. To, and R. Noufi, Prog. Photovolt. **16**, 235 (2008).

[2]   M.A. Green, K. Emery, Y. Hishikawa, and W. Warta, Prog. Photovolt: Res. Appl. **17**, 85 (2009).

[3]   M.A. Contreras, K. Ramanathan, J. AbuShama, F. Hasoon, D. L. Young, B. Egaas, and R. Noufi, Prog. Photovolt.: Res. Appl. **13**, 209 (2005).

[4]   J.H. Scofield, J. Electron Spectrosc. Relat. Phenom. **8**, 129 (1976).

[5]   J.R. Tuttle, D.S. Albin, and R. Noufi, Sol. Cells **30**, 21 (1991); D. Schmid, M. Ruckh, F. Grunwald, and H.-W. Schock, J. Appl. Phys. **73**, 2902 (1993).

[6]   M. Morkel, L. Weinhardt, B. Lohmüller, C. Heske, E. Umbach, W. Riedl, S. Zweigart, and F. Karg, Appl. Phys. Lett. **79**, 4482 (2001).

[7]   M. Bär, S. Nishiwaki, L. Weinhardt, S. Pookpanratana, O. Fuchs, M. Blum, W. Yang, J. D. Denlinger, W.N. Shafarman, and C. Heske, Appl. Phys. Lett. **93**, 244103 (2008).

[8]   M. Bär, W. Bohne, J. Röhrich, E. Strub, S. Lindner, M. C. Lux-Steiner, Ch.-H. Fischer, T. P. Niesen, and F. Karg, J. Appl. Phys. **96**, 3857 (2004).

[9]   B.L. Henke et al., *Atomic Data and Nuclear Data Tables* **54**, 181 (1993); http://www-cxro.lbl.gov/optical _constants/atten2.html.

[10] C. Heske, D. Eich, R. Fink, E. Umbach, T. van Buuren, C. Bostedt, L. J. Terminello*, S. Kakar, M. M. Grush, T. A. Callcott, F. J. Himpsel, D. L. Ederer, R. C. C. Perera*, W. Riedl, and F. Karg, Appl. Phys. Lett. **74**, 1451 (1999).

[11] Ch. Barglik-Chory et al., Chem. Phys. Lett. **379**, 443 (2003).

[12] L. Weinhardt, M. Morkel, Th. Gleim, S. Zweigart, T.P. Niesen, F. Karg, C. Heske, and E. Umbach, Proc. 17th European Photovoltaic Solar Energy Conference, October 2001, Munich, p. 1261.

[13] L. Weinhardt, O. Fuchs, D. Groß, G. Storch, E. Umbach, N.G. Dhere, A.A. Kadam, S.S. Kulkarni, and C. Heske, Appl. Phys. Lett. **86**, 062108 (2005).

[14] S. Nishiwaki et al.,WCPEC-4, Waikoloa, HI, 2006, p. 416.

[15] V. Kumar et al., Opt. Mater. **12**, 115 (1999).

[16] W. Hörig et al., Thin Solid Films **48**, 67 (1978).

[17] D. Briggs et al., *Practical Surface Analysis by Auge rand X-ray Spectroscopy,* John Wiley & Sons Ltd., New York (1983).

[18]   L. Weinhardt, O. Fuchs, A. Peter, E. Umbach, C. Heske, J. Reichardt, M. Bär, I. Lauermann, I. Kötschau, A. Grimm, S. Sokoll, T.P. Niesen, S. Visbeck, and F. Karg, J. Phys. Chem. **124**, 074705 (2006).

[19]   C. Heske, D. Eich, R. Fink, E. Umbach, T. van Buuren, C. Bostedt, S. Kakar, L. J. Terminello, M. M. Grush, T. A. Callcott, F. J. Himpsel, D. L. Ederer, R. C. C. Perera, W. Riedl, and F. Karg, Surf. Interface Anal. **30**, 459 (2000).

[20]   L. Weinhardt, O. Fuchs, A. Peter, E. Umbach, C. Heske, J. Reichardt, M. Bär, I. Lauermann, I. Kötschau, A. Grimm, S. Sokoll, T.P. Niesen, S. Visbeck, and F. Karg, J. Chem. Phys. **124**, 074705 (2006).

[21]   Th. Glatzel, D. Fuertes Marron, Th. Schedel-Niedrig, S. Sadewasser, and M. Ch. Lux-Steiner, Appl. Phys. Lett. **81**, 2017 (2002).

[22]   V. Probst, W. Stetter, W. Riedl et al., Thin Solid Films **387**, 262 (2001).

[23]   N. Kohara, S. Nishiwaki, Y. Hashimoto, T. Negami, and T. Wada, Sol. Energy Mater. Sol. Cells **67**, 209 (2001).

[24]   R. Scheer and H.-J. Lewerenz, J. Vac. Sci. Technol. A **13**, 1924 (1995).

[25]   D. Schmid, J. Kessler, and H. W. Schock, Proceedings of the 12th European Photovoltaic Solar Energy Conference, Amsterdam, 653 (1994).

[26]   D. Schmid et al., J. Appl. Phys. **73**, 2902 (1993).

[27]   R. Schaffler et al., Diffusion and Defect Data B **51-52**, 347 (1996).

[28]   A. J. Nelson, D. Niles, L. L. Kazmerski, D. Rioux, R. Patel, and H. Höchst, J. Appl. Phys. **72**, 976 (1992).

[29]   W. N. Shafarman and J. E. Phillips, Proceedings of the 25th IEEE Photovoltaic Specialists Conference, Washington, DC, 1996, p. 917.

[30]   P. E. Russell, O. Jamjoum, R. K. Ahrenkiel, L. L. Kazmerski, R. A. Mickelsen, and W. S. Chen, Appl. Phys. Lett. **40**, 995 (1982).

[31]   W. Jaegermann, T. Löher, and C. Pettenkofer, Cryst. Res. Technol. **31**, 273 (1996).

[32]   J. Pouzet, H. Hadouda, J. C. Bernede, and R. Le Ny, J. Phys. Chem. Sol. **57**, 1363 (1996).

Presentations (contributed oral presentations, unless marked as "poster" or "invited oral")

T1. M. Bär, "Formation of the buffer/CuInS$_2$ interface", WCPEC-4, Hawaii, May 2006.

T2. L. Weinhardt, "Unfavorable band alignment at the CdS/Cu(In,Ga)S2 interface in thin film solar cells", WCPEC-4, Hawaii, May 2006.

T3. C. Heske, "Chemical and electronic properties of the CdS/Cu(In,Ga)(S,Se)$_2$/Mo junctions in thin film solar cells", EMRS2006, Nice, France, May 2006.

T4. C. Heske, "Surface and interface analysis in Las Vegas", Seminar Experimentelle Physik II, University of Würzburg, Germany, July 20, 2006 (invited oral).

T5. C. Heske, "Characterizing surfaces and interfaces in thin film solar cells by soft X-ray spectroscopy", Symposium: Photovoltaic, Solar Energy Materials and Thin Films, XV International Materials Research Congress, Cancun, Mexico, August 2006 (invited oral).

T6. C. Heske, "How to reveal the chemical and electronic properties of interfaces, buried layers, and liquids with soft x-ray spectroscopy", Materials Science and Engineering Department, Stanford University, August 31, 2006 (invited oral).

T7. C. Heske, "How to reveal the chemical and electronic properties of interfaces, buried layers, and liquids with soft x-ray spectroscopy", Physics Department, Boston University, December 8, 2006 (invited oral).

T8. M. Bär, "Chemical and Electronic Properties of the Front and Back Surfaces of Chalcopyrite Thin Film Solar Cell Absorbers", 2007 MRS Spring Meeting, San Francisco, April 2007.

T9. L. Weinhardt, "X-ray and electron spectroscopy investigation of interfaces and surfaces in CdTe thin film solar cells", 2007 MRS Spring Meeting, San Francisco, April 2007.

T10. J. Zhou (NREL), "The mechanism of J-V "roll-over" in CdS/CdTe devices", 2007 MRS Spring Meeting, San Francisco, April 2007.

T11. C. Heske, "Introduction" at the Young Scientist Tutorial, 2007 MRS Spring Meeting, San Francisco, April 2007 (invited oral).

T12. M. Bär, L. Weinhardt, "Surface/interface characterization and modification" at the Young Scientist Tutorial, 2007 MRS Spring Meeting, San Francisco, April 2007 (invited oral).

T13. C. Heske, "Characterization of the electronic and chemical structure at Cu(In,Ga)(S,Se)$_2$ and CdTe thin film solar cell interfaces", 2007 Solar Review Meeting, Denver, April 2007 (poster).

T14. C. Heske, "Surface and Interface Analysis of Real-World Cu(In,Ga)(S,Se)$_2$ Thin Film Solar Cells", Global Solar, Tucson, AZ, July 2007.

T15. M. Bär, "Bandoffset Tailoring – A Tool To Improve Thin Film Solar Cells", Hahn-Meitner-Institute, Berlin, July 2007 (invited oral).

T16. M. Bär, "Surface, bulk, and interface properties of $Cu(In,Ga)Se_2$-based thin film solar cell structures, 15th International Conference on Vacuum Ultraviolet Radiation Physics, Berlin (Germany), July 29 – August 3, 2007 (poster).

T17. M. Bär, "The chemical structure of the $CdS/Cu(In,Ga)Se_2$ interface in high-efficiency thin film solar cells", 22nd European Photovoltaic Solar Energy Conference, Milan (Italy), September 3-7, 2007.

T18. M. Bär, "Improving Thin Film Solar Cells by Deliberate Interface Tailoring", Auswahlsitzung Helmholtz-Gemeinschaft Berlin, November 2007 (invited oral).

T19. M. Bär, "Bandoffset Tailoring – A Tool To Improve Thin Film Solar Cells", Physikalisches Kolloquium, Brandenburgische Technische Universität Cottbus, April 2008 (invited oral).

T20. M. Bär, "Depth-dependent band gap energies in chalcopyrite thin film solar cell absorbers", 33rd IEEE Photovoltaic Specialists Conference, San Diego (CA), USA, May 11-16, 2008.

T21. C. Heske, "Soft x-ray spectroscopy of the $Cu(In,Ga)(S,Se)_2/Mo$ back contact interface", European Materials Research Society Spring Meeting, Strasbourg, France, May 26-30, 2008 (invited oral).

T22. M. Bär, "Spectroscopic Characterization of Thin Films Used in Energy Conversion Devices", American Chemical Society 42nd Western Regional Meeting, Las Vegas, USA, September 22-26, 2008 (invited oral).

T23. M. Bär, "How soft x-ray spectrosocpies can help to improve thin film solar cells", Berufungsvortrag, Brandenburgische Technische Universität Cottbus, February 2009 (invited oral).

T24. M. Bär, "How soft x-ray spectroscopies can help to reveal the secrets of chalcopyrite-based thin film solar cells", Spring Meeting of the Materials Research Society, San Francisco (CA), USA, April 13-17, 2009 (invited oral).

T25. C. Heske, "Introduction" at the Young Scientist Tutorial, 2009 MRS Spring Meeting, San Francisco, April 13, 2009 (invited oral).

T26. S. Pookpanratana, "Spectroscopic Analysis of the Chemical Structure at the $CdS/Cu(In,Ga)Se_2$ Interface in High-Efficiency Solar Cell Devices", 34th IEEE Photovoltaic Specialists Conference, Philadelphia (PA), USA, June 7–12, 2009.

T27. Xiangxin Liu (U of Toledo), "Migration and Oxidation of Sulfur at the Back Contact in CdTe Cells", 34th IEEE PVSC, Philadelphia, PA, June 7-12, 2009.

T28. M. Bär, "Chemical structure of the CdS/CuGaSe$_2$ interface – pushing the limit of depth-resolved analysis by soft x-ray emission spectroscopy", E-MRS Spring Meeting 2009, Strasbourg, France, June 8-12, 2009 (poster).

Publications

Deliverables:
1st year – one or more submitted conference articles
2nd year – a submitted journal and one or more submitted conference articles
3rd year – a submitted journal and >1 submitted conference articles

P1. Conference: "Chemical bath deposition of CdS thin films on CuInS$_2$ and Si substrates – a comparative x-ray emission study", M. Bär, L. Weinhardt, O. Fuchs, J. Klaer, J. Peiser, H.-W. Schock, E. Umbach, and C. Heske, Proceedings 4th World Conference on Photovoltaic Energy Conversion (WCPEC), Waikoloa, Hawaii, May 2006, p. 416-419.

P2. Conference: "Comparison of band alignments at various CdS/Cu(In,Ga)(S,Se)$_2$ interfaces in thin film solar cells", L. Weinhardt, O. Fuchs, D. Groß, G. Storch, N.G. Dhere, A.A. Kadam, S.S. Kulkarni, C. Heske, and E. Umbach, Proceedings 4th World Conference on Photovoltaic Energy Conversion (WCPEC), Waikoloa, Hawaii, May 2006, p. 412-415.

P3. Journal: "Surface modifications of Cu(In,Ga)S$_2$ thin film solar cell absorbers by KCN and H$_2$O$_2$/H$_2$SO$_4$ treatments", L. Weinhardt, O. Fuchs, D. Groß, E. Umbach, C. Heske, N.G. Dhere, A.A. Kadam, and S.S. Kulkarni, J. Appl. Phys. **100**, 024907 (2006).

P4. Conference/Journal: "Chemical properties of the Cu(In,Ga)Se$_2$/Mo/glass interfaces in thin film solar cells", L. Weinhardt, M. Blum, M. Bär, C. Heske, O. Fuchs, E. Umbach, J.D. Denlinger, K. Ramanathan, and R. Noufi, Thin Solid Films **515**, 6119-6122 (2007) (Proceedings EMRS2006, Nice, France, May 2006).

P5. Conference: "The mechanism of J-V "roll-over" in CdS/CdTe devices", J. Zhou, X. Wu, Y. Yan, S. Asher, J. L. F. Da Silva, Su-Huai Wei, L. Weinhardt, M. Bär, and C. Heske, "Thin-Film Compound Semiconductor Photovoltaics – 2007", Materials Research Society Symposium Proceedings, San Francisco, April 2007, Vol. 1012, p. 491-496.

P6. Conference: "Band Gap Energy of Chalcopyrite Thin Film Solar Cell Absorbers Determined by Soft X-Ray Emission and Absorption Spectroscopy", M. Bär, L. Weinhardt, S. Pookpanratana, C. Heske, S. Nishiwaki, W. Shafarman, O. Fuchs, M. Blum, W. Yang, and J.D. Denlinger, Proc. 33rd IEEE Photovoltaic Specialists Conference, San Diego (CA), USA, May 11-16, 2008.

P7. Journal: "Depth-resolved band gap in Cu(In,Ga)(S,Se)$_2$ thin films", M. Bär, S. Nishiwaki, L. Weinhardt, S. Pookpanratana, O. Fuchs, M. Blum, W. Yang, J.D. Denlinger, W.N. Shafarman, and C. Heske, Appl. Phys. Lett. **93**, 244103 (2008).

P8.   Journal: "Chemical structures of the Cu(In,Ga)Se$_2$/Mo and Cu(In,Ga)(S,Se)$_2$/Mo interfaces", M. Bär, L. Weinhardt, C. Heske, S. Nishiwaki, and W. N. Shafarman, Phys. Rev. B **78**, 075404 (2008).

P9.   Journal: "Electronic level alignment at the deeply buried absorber/Mo interface in chalcopyrite-based thin film solar cells", M. Bär, S. Nishiwaki, L. Weinhardt, S. Pookpanratana, W. N. Shafarman, and C. Heske, Appl. Phys. Lett. 93, 042110 (2008).

P10. Journal: "Resonant inelastic soft x-ray scattering map of CdS", L. Weinhardt, O. Fuchs, A. Fleszar, M. Bär, M. Blum, M. Weigand, J.D. Denlinger, W. Yang, W. Hanke, E. Umbach, and C. Heske, Phys. Rev. B **79**, 165305 (2009).

P11. Journal: "Chemical and electronic surface structure of 20%-efficient Cu(In,Ga)Se$_2$ thin film solar cell absorbers", M. Bär, I. Repins, M.A. Contreras, L. Weinhardt, R. Noufi, and C. Heske, Appl. Phys. Lett., in print.

P12. Conference (submitted to Proc. 34th IEEE PVSC): "Spectroscopic Analysis of the Chemical Structure at the CdS/Cu(In,Ga)Se$_2$ Interface in High-Efficiency Solar Cell Devices", S. Pookpanratana, I. Repins, M. Bär, R. Félix, M. Blum, L. Weinhardt, W. Yang, J.D. Denlinger, M.A. Contreras, and C. Heske

P13. Conference (submitted to Proc. 34th IEEE PVSC): "Migration and Oxidation of Sulfur at the Back Contact in CdTe Cells", Xiangxin Liu (U Toledo), A.D. Compaan, Kai Sun, L. Weinhardt, M. Bär, S. Pookpanratana, C. Heske, O. Fuchs, W. Yang, and J.D. Denlinger

Other deliverable: "A solar cell (manufactured by one of the partners within the TFPPP) with novel attributes where the junction were engineered according to Subcontractor's recommendation"

The fulfilment of this deliverable was pursued with several partners in parallel: K. Ramanathan (NREL), X. Wu (NREL), M. Beck (Global Solar), K. Ramanathan (Miasolé), M. Beck (Solyndra), and U. Schoop (Global Solar). Due to the unexpected termination of the TFPPP program on 9/30/2006 (i.e., after 16 months after the receipt of first funds in our project) and significant changes in personnel and goals of the various partners, this deliverable could not be achieved. Nevertheless, substantial insights into various interfaces of CuInGaSe$_2$- and CdTe-based solar cells could be obtained and were (are) published in the openly accessible literature and presented at pertinent conferences, such that the results can be easily incorporated into the processes at former TFPPP and other partners.

REPORT DOCUMENTATION PAGE		*Form Approved* *OMB No. 0704-0188*

The public reporting burden for this collection of information is estimated to average 1 hour per response, including the time for reviewing instructions, searching existing data sources, gathering and maintaining the data needed, and completing and reviewing the collection of information. Send comments regarding this burden estimate or any other aspect of this collection of information, including suggestions for reducing the burden, to Department of Defense, Executive Services and Communications Directorate (0704-0188). Respondents should be aware that notwithstanding any other provision of law, no person shall be subject to any penalty for failing to comply with a collection of information if it does not display a currently valid OMB control number.
PLEASE DO NOT RETURN YOUR FORM TO THE ABOVE ORGANIZATION.

1. **REPORT DATE** *(DD-MM-YYYY)* September 2009	2. **REPORT TYPE** Subcontractor Report	3. **DATES COVERED** *(From - To)* June 2005 - June 2009	
4. **TITLE AND SUBTITLE** Characterization of the Electronic and Chemical Structure at the Thin Film Solar Cell Interfaces		5a. **CONTRACT NUMBER** DE-AC36-08-GO28308	
		5b. **GRANT NUMBER**	
		5c. **PROGRAM ELEMENT NUMBER**	
6. **AUTHOR(S)** C. Heske		5d. **PROJECT NUMBER** NREL/SR-520-46434	
		5e. **TASK NUMBER** PVB91110	
		5f. **WORK UNIT NUMBER**	
7. **PERFORMING ORGANIZATION NAME(S) AND ADDRESS(ES)** University of Nevada, Las Vegas Las Vegas, Nevada 89154-4003		8. **PERFORMING ORGANIZATION REPORT NUMBER** XXL-5-44205-12	
9. **SPONSORING/MONITORING AGENCY NAME(S) AND ADDRESS(ES)** National Renewable Energy Laboratory 1617 Cole Blvd. Golden, CO 80401-3393		10. **SPONSOR/MONITOR'S ACRONYM(S)** NREL	
		11. **SPONSORING/MONITORING AGENCY REPORT NUMBER** NREL/SR-520-46434	
12. **DISTRIBUTION AVAILABILITY STATEMENT** National Technical Information Service U.S. Department of Commerce 5285 Port Royal Road Springfield, VA 22161			
13. **SUPPLEMENTARY NOTES** NREL Technical Monitor: Bolko von Roedern			

14. **ABSTRACT** *(Maximum 200 Words)*

This project was devoted to deriving the electronic structure of interfaces in Cu(In,Ga)(S,Se)2 and CdTe thin-film solar cells. By using a unique combination of spectroscopic methods (photoelectron spectroscopy, inverse photoemission, and X-ray absorption and emission), a comprehensive picture of the electronic (i.e., band alignment in the valence and conduction band) as well as chemical structure can be painted. The work focused on the following: (1) deriving the benchmark picture for world-record cells, (2) analyzing state-of-the-art cells from industrial processes, and (3) troubleshooting of cells with substandard performance.

15. **SUBJECT TERMS**
PV; CIGSS; CdTe; electronic structure; interfaces; thin film; solar cells; photoelectron spectroscopy; inverse photoemission; X-ray absorption and emission;

16. **SECURITY CLASSIFICATION OF:**			17. **LIMITATION OF ABSTRACT**	18. **NUMBER OF PAGES**	19a. **NAME OF RESPONSIBLE PERSON**
a. **REPORT** Unclassified	b. **ABSTRACT** Unclassified	c. **THIS PAGE** Unclassified	UL		19b. **TELEPHONE NUMBER** *(Include area code)*

Standard Form 298 (Rev. 8/98)
Prescribed by ANSI Std. Z39.18

F1146-E(10/2008)